ORIGINAL ARTICLE

Removal of water-soluble lignin model pollutants with graphene oxide loaded ironic sulfide as an efficient adsorbent and heterogeneous Fenton catalyst

Junjian An [a,b], Shanshan Wang [a], Mengxuan Huang [a], Jian Zhang [b], Peng Wang [a,*]

[a] *Hubei provincial Key Laboratory of Green Materials for Light Industry, School of Materials and Chemical Engineering, Hubei University of Technology, Wuhan 430068, PR China*
[b] *Guangxi Key Laboratory of Clean Pulp & Papermaking and Pollution Control, College of Light Industry and Food Engineering, Guangxi University, Nanning 530004, PR China*

Abstract Advanced oxidation processes (AOPs) have gained extensive attentions in organic decontamination in past decades. Iron-contained compound is an interesting material due to its adsorptive and catalytic performance, which has been applied widely in AOPs. Thus, graphene oxide (GO)-Fe_3S_4 composite was synthesized by a solvothermal process and assessed as an effective adsorptive and catalytic dual functional material in this work. The composite displayed prominent adsorptive and heterogeneous Fenton-like catalytic performance, which was affected by preparation condition and the reactive parameters in catalytic system. Under optimized reactive conditions, the GO-Fe_3S_4 composite yielded rapid degradation of vanillic acid, which the corresponding apparent rate constant was 1.81×10^{-1} min^{-1}. Catalytic mechanism analysis revealed that the main oxygen species was hydroxyl radicals bounded on the surface of the composite. And the generation of $\bullet O_2^-$ was contributed to the conversion of H_2O_2 to $\bullet OH$. The analysis of degradation intermediates of vanillic acid and *p*-hydroxybenzoic showed that these compounds could be mineralized to small molecules. The prominent enhanced heterogeneous Fenton-like catalytic performance of GO-Fe_3S_4 was due to a larger specific surface area, plenty of reductive active sites in the composite and a high mass transfer efficiency of oxidizing radicals in the reactive system.

* Corresponding author.
 E-mail address: ahwp1234@163.com (P. Wang).

1. Introduction

Lignin and its degradation products generated from pulping and papermaking factories cause severe harm to aquatic life and have aroused extensive environmental concern. The alkali recovery process is a traditional technology for removal of lignin from pulping and papermaking wastewater. However, this method can only remove the insoluble lignin and there is still a large amount of water-soluble degradation products of lignin existed in the pulping and papermaking wastewater. In traditional treatment process, the wastewater generally undergoes primary sedimentation and secondary biochemical treatment. Researchers have found that papermaking effluent discharged from secondary biochemical treatment contained abundant aromatic compounds and alkanes which were mainly originated from lignin. And aromatic compounds were mainly existed in the form of single benzene ring, which caused severe environmental problems related to their high COD (Chemical Oxygen Demand) together with deep color content (as shown in Fig. 1) (Ma Li Hua and Wan Jin Quan 2013). In addition, they are stable in structure and exhibited stronger biotoxicity, which made them hardly be degraded through biological treatment. With the increasingly stringent environmental protection policies, it's urgent to dispose these aromatic compounds with high degradation and mineralization efficiency.
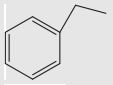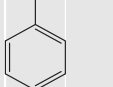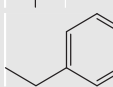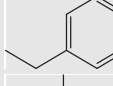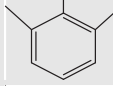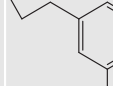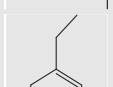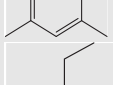
In last decades, many research studies have been focused on disposing lignin and its degraded products from pulp mill wastewater. Traditional physical methods (such as microwave method and ultrasonic method) can destroy the chemical structure of C_α-C_β in basic structural unit of phenylpropane in lignin molecules (M.W.I. Schmidt et al., 1997). However, these methods consume energy and produce noise,

resulting in increased economic cost and an adverse health effect. The chemical processes (hydrogenation reduction, catalytic oxidation and electrochemical method) could transform lignin molecules to low molecule weight products (M.P. Pandey and C.S. Kim 2011, Ha et al., 2019). Nevertheless, the processes faced the challenges of low degradation efficiency, limited activity ability, uncertain active catalytic sites and weak selectivity (Parpot et al., 2000). Biological processes have also been investigated to degrade lignin by microorganism, such as white rot fungi (Fernandez-Fueyo et al., 2012). brown rot fungi, bacillus amyloliquefaciens (Mei et al., 2020), mixed bacteria (Sen et al., 2020) and mimic enzymes (Zeng et al., 2015; Schutyser et al., 2018; Cooper et al., 2020). The processes demand high culture conditions of strain. Except that, the repeatability of treatment efficiency was obvious poor, which limited the practical application of this process. Advanced oxidation processes (AOPs), as a promising technology, are expected to solve the above problems. The traditional Fenton process can be utilized to remove lignin pollutants (Bentivenga et al., 2003, Torrades et al., 2011). Besides hydroxyl radicals, sulfate radicals ($Fe^{2+}/S_2O_8^{2-}$–H_2O_2 system) was also employed to dispose the aromatic compounds generated from lignin in the effluent discharged from secondary biochemical treatment process (Ma Li Hua and Wan Jin Quan 2013). As showed in Table 1, it was found that the aromatic compounds could be degraded at a certain extent. However, the degradation efficiency was relatively low (21 %∼52 %). This mainly because the aromatic compounds concentration was fairly low which induced the long distance between the active species and pollutants. Due to the limited lifetime of oxidative active species (•OH < 1 μs; $SO_4^{·-}$: 4 s), they may lose their activation before reach the pollutants. Therefore, the degradation efficiency was poor in the
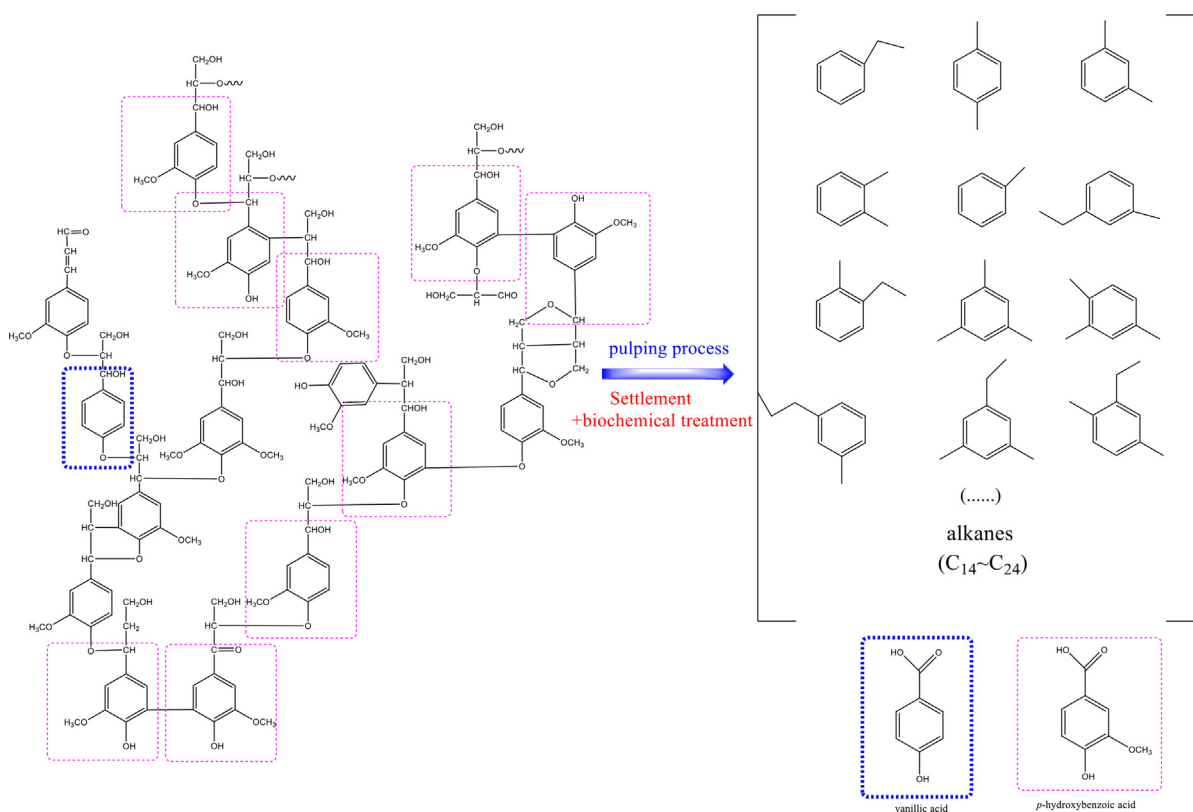
Fig. 1 The main structure of softwood lignin (Laurichesse and Avérous 2014), lignin degradation products after biochemical treatment and their model compounds (vanillic acid and *p*-hydroxybenzoic acid).

Table 1 Changes of part aromatic compounds in secondary effluent of papermaking wastewater before and after homogeneous Fenton process ($Fe^{2+}/S_2O_8^{2-}$–H_2O_2 system) (Ma Li Hua and Wan Jin Quan 2013).

Number	Pollutants	Secondary effluent / %	Tertiary effluent / %
1		6.57	3.23
2		13.70	9.56
3		6.89	4.56
4		13.90	10.81
5		4.56	2.15
6		1.45	0.98
7		2.13	1.67
8		1.13	0.67

above homogeneous Fenton process, especially for the removal of low concentration pollutants. In addition that, the narrow application pH range (pH < 3) and iron sludge problem further restricted the practice application of homogeneous Fenton process. In order to enhance the degradation efficiency of lignin, ultraviolet light (UV) is introduced to Fenton reaction. And TiO_2 (Ma et al., 2008), ZnO (Yeber, et al., 2000, Kansal et al., 2008) and other photocatalysts could also remove lignin molecules with the irradiation of UV or visible light. However, the deep color of lignin-contained water was adverse to the absorption and utilization of UV or visible light in reactive system, reducing the disposal efficiency of lignin. Compared to homogeneous Fenton process, heterogeneous Fenton process exhibits expansive application prospect due to the advantages of wide application pH range, avoiding the generation of iron sludge and recycle of catalysts. Iron contained compounds, e.g. iron oxides (Fe_2O_3 (Huang et al., 2019), Fe_3O_4 (Xu and Wang 2012, Chen et al., 2017)), iron hydroxides (FeOOH (Hou et al., 2017, Qian et al., 2017)), and iron hypochlorites (FeOCl (Yang et al., 2013, Sun et al., 2018, Zhang et al., 2020, Han and Gao 2008)) are widely investigated as catalysts in heterogeneous Fenton system. Unfortunately, the activities of these catalysts are not good enough to degrade persistent organic pollutants efficiently. Considering the low concentration of lignin degradation intermediate products in papermaking effluent, it may be more effective to gather the molecules of these pollutants firstly and then attack them by oxidizing active species. In this sense, the strategy of adsorption-degradation

process in heterogeneous Fenton system may be more successful to remove the lignin degradation products with light concentration. Hence, it is urgent to seek materials with high adsorption and heterogeneous Fenton catalytic performance to remove the water-soluble lignin from wastewater.

Iron sulfides, existed extensively in natural world, play an important part in the inchoate element cycles of carbon, nitrogen, oxygen and sulfur (Rickard and Luther 2007, Han and Gao 2008). As a kind of typical iron sulfide, greigite (Fe_3S_4) exhibited superior catalytic reduction activity in the fields of CO_2 catalytic reduction (Roldan and de Leeuw 2016), heavy metal disposal (Kong et al., 2015) and N_2 fixation (Zhao et al., 2018). On account of the plentiful reductive sites on the surface of Fe_3S_4, this compound could activate H_2O_2 for the degradation of organic contaminant. And the reconstruction of Fe_3S_4 surface through the reaction between the discharged Fe and S species sustained a stable •OH production during the heterogeneous Fenton process. However, the released species of S and Fe(II) on Fe_3S_4 surface can likewise be oxidized by the in-situ generated •OH to higher valence state, leading to the decrease of the active Fe(II) matter on the surface of this compound. Thus, the iron redox cycle becomes weaker, resulting in lower catalytic efficiency. Therefore, it is critical to consume the superfluous oxidizing radicals on the surface of Fe_3S_4 before the over-oxidation of Fe(II) species. In consideration of the surface reaction in heterogeneous Fenton process, the mass transfer efficiency of oxidizing radicals generated on the catalyst surface to the pollutants mainly existed in bulk solution is a key role in the degradation of organic contaminants. And high transfer efficiency of •OH radicals from Fe_3S_4 surface to pollutants can also prevent the oxidation of S and Fe(II) on the surface of the catalyst.

Carbon-based materials, for instance graphite, activate carbon, carbon nanotubes, carbon nanofibers and graphene, could be utilized as high-performing catalyst carriers during the process of heterogeneous catalytic reaction (Jiang et al., 2010, Thakur et al., 2010, Jiménez et al., 2011, An et al., 2013). Among them, graphene oxide (GO) is a typical carbon materials, which exhibit two-dimension cycle planer structure. By the introducing of GO, many complex catalysts with particular structure (such as self-assembled GO nanostructures) were prepared (Guo et al., 2017, Deng et al., 2021, Xu et al., 2021), which exhibited excellent catalytic performance in fields of organic pollutants degradation and hydrogen production. As an outstanding catalyst support, GO could provide abundant adsorption sites for pollutants. Differ from graphene, abundant oxygenous groups, for instance carboxyl groups and hydroxyl groups, are existed on the surface of GO, which exhibit a good affinity to water and are favorable to be dispersed in water solution. The hydrophilic groups of GO make it easy to absorb water-soluble pollutants via the formation of chemical bonds, e.g., such as hydrogen bonds and other physical interaction.

Although the structure of lignin is complex, its molecule is mainly composed of guaiacyl, syringyl and p-hydroxyphenyl groups. As previously mentioned, lignin macromolecules are degraded to many kinds of hydrosoluble aromatic substances after the pulping process and subsequent biochemical treatment, which are basically derived from the basic structural units of lignin. Therefore, researchers often evaluate the application value of catalytic system to treat pulping and papermaking wastewater by studying the degradation of monomer model compounds of lignin. Fig. 1 exhibited the structure of lignin in coniferous wood, the main raw material for papermaking, which is mainly composed of guaiacyl and a small amount of p-hydroxyphenyl structural units. Therefore, vanillic acid and p-hydroxybenzoic acid were selected as the model pollutants of lignin in this study. And GO-Fe_3S_4 composites were prepared with solvothermal method, planning to exploit high performance adsorption and heterogeneous Fenton catalysts. The composites may adsorb these compounds through hydrogen-interaction and π-π stacking effect, which improved the transfer efficiency of •OH radicals from catalyst surface to target pollutants. Thus, the over-oxidation of active ferrous species on the catalyst surface can be avoided, leading to the high and stable catalytic activity in heterogeneous process. The H_2O_2 consumption efficiency,

the generated oxidative species and the intermediate products of the model compounds were probed in detail to explore and evaluate the possible heterogeneous Fenton catalytic mechanisms and degradation efficiency of GO-Fe$_3$S$_4$. The GO-Fe$_3$S$_4$-H$_2$O$_2$ catalytic system was further applied to dispose effluent discharged from the secondary biochemical process in pulping and papermaking mills to farther evaluate its potential application value in practical. And the reusability of GO-Fe$_3$S$_4$ was also investigated for its practical application. This work not only provide an effective strategy to dispose the degradation products of lignin in papermaking effluent after settlement and biochemical process, but also possess the potential application prospect to remove low concentration nonbiodegradable organic pollutants efficiently in wastewater.

2. Experimental

2.1. Chemicals and materials

Iron(III) chloride hexahydrate (FeCl$_3$·6H$_2$O), thiourea, ethylene glycol, absolute ethyl alcohol, potassium iodide, vanillic acid and p-hydroxybenzoic acid (PHBA) were acquired from Sinopharm Chemical Reagent Co., ltd. (China). Hydrogen peroxide, hydrochloric acid, Superoxide dismutase (SOD, specific activity of $\geq$ 2500 units mg^{-1}) and Sodium hydroxide were obtained from Aladdin Chemistry Co., ltd. (China). All chemicals utilized in this work were of analytic grade.

2.2. Preparation of GO-Fe$_3$S$_4$ composites

The graphene oxide (GO) was prepared in accordance with the means of Hummers and Offeman (W. Hummers and R. Offeman 1958), and GO-Fe$_3$S$_4$ composite was obtained with a solvothermal process. Firstly, stoichiometric ratios of thiourea and FeCl$_3$·6H$_2$O were dissolved in the solution of ethylene glycol and deionized water (V$_{glycol}$:V$_{water}$ = 3:1), followed by magnetic agitation. A certain amount of GO (0–8 %) was added to the aforesaid solution under magnetic agitation. Then, the resulting dispersion liquid was shifted to a Teflon-lined stainless steel vessel and was heated at 180 ℃ for 9 h. Afterwards, the dispersion was cooled down to indoor temperature, and the suspension was centrifuged immediately followed by sequential washing with ethanol and deionized water for at least three times. In the end, the gathered precipitate was heated in an oven at 60 ℃ for 6 to 12 h and then received as the GO-Fe$_3$S$_4$ composite.

2.3. Adsorption experiment

The adsorption process was conducted by dispersing GO-Fe$_3$S$_4$ composite in the solution of lignin model pollutants (35 mg/L) at pH 4.0. At opportune time intervals, a certain amount of the dispersion liquid (about 3 mL) were taken out, and promptly centrifuged at 14000 rpm with a centrifugal (EBA-21, Hettich, Germany). The supernatant was further filtered through a 0.22 μm pore size filter for further analysis.

2.4. Degradation experiment

The degradation reaction was carried out in a conical flask at 25℃. Typically, a specified amount of GO-Fe$_3$S$_4$ composite was immersed to a solution of vanillic acid (50 mL; 35 mg/ L) or p-hydroxybenzoic acid (50 mL; 25 mg/L) by sonicating for 5 min, followed by adjusting pH value to a certain value. The suspension was agitated for 2 h to reach the equilibrium of adsorption/desorption between the catalyst and substrate. Aliquot of the dispersion was taken out and promptly centrifuged at 14000 rpm. The concentration of substrate in the supernatant was monitored and taken as its original concentration. Then, H$_2$O$_2$ was added to the dispersion under the condition of stirring. At given times, quantitative dispersion liquids (about 3 mL) were transferred to a centrifugal tube which contained a certain amount of absolute ethyl alcohol (to quench •OH radicals) and centrifuged. The substrate concentration was measured promptly.

2.5. Characterization and analysis of catalysts

Surface morphology of Fe$_3$S$_4$, graphene oxide (GO) and GO-Fe$_3$S$_4$ composite were detected by a ZEISS Gemini 300 scanning electron microscope (SEM). The crystal structure of catalysts was analyzed through X-ray diffraction (XRD), which was conducted on a Bruker D8 Advance diffractometer coupled with Cu Ka radiation and a diffracted beam graphite monochromator. X-ray photoelectron spectroscopy (XPS) detection was carried out on a VG Multilab 2000 X-ray photoelectron spectrometer. And Mg Ka X-ray was selected as the excitation source. Brunauer-Emmett-Teller (BET) surface areas were explored by N$_2$ adsorption–desorption at 77 K with a MICROMETERS ASAP 2020 apparatus. The chemical structure was explored on a Fourier transform infrared spectroscopy (FT-IR) in the scanning range of 4000 $\sim$ 400 cm^{-1}. The magnetic properties (M−H curve) of Fe$_3$S$_4$ and GO-Fe$_3$S$_4$ composite were detected at 300 K with an ADE 4HF vibrating sample magnetometer. Raman spectra were measured by a Thermo Scientific DXR Raman spectrometer at 532 nm excitation wavelength.

The concentrations of vanillic acid and PHBA were detected with high-performance liquid chromatography (HPLC) on a HPLC system which composed of Jasco PU-2089 quaternary gradient pumps with Jasco UV-2075 Intelligent and UV/Visible light (Vis) detector. The system was also equipped with an automatic sample injector (Rheodyne, Cotati, CA, USA) with a 20-μL loop. An amethyst C18-P column (5 μm, 4.6 × 250 mm) was employed as separation column. In HPLC experiments, a mixture of methanol and 1 % glacial acetic acid (60:40, v/v) was used as mobile phase for vanillic acid. And the mobile phase for PHBA was composed of methanol and 0.2 % phosphoric acid solution (40:60, v/v). The flow rate of the above mobile phase was both 1.0 mL min^{-1}. It was filtered through 0.2 μm filter prior to use. The detected UV wavelength was 260 and 254 nm for vanillic acid and PHBA, respectively. A liquid chromatograph (LC, Agilent 1100) coupled with a mass spectrometer (MS) (Agilent 5975, Agilent Technologies, Wilmington, DE) was used to explore the chemical structure of the degradation products of vanillic acid and PHBA. An amethyst C18-P column (5 μm, 4.6 × 250 mm) was selected as the separation column. The mobile phase was a mixture of water and methanol (85:15, v/v) with a flow rate of 0.8 mL min^{-1}. The eluent was filtered through a 0.2 μm filter prior to use. The ratio of m/e was from 50 to 300 and the model was confirmed as negative ion style·H$_2$O$_2$ was determined with the DPD method (H. Bader

et al., 1988). The concentration of •OH generation was detected by employing the coumarin probe method (Guan et al., 2008).

3. Results and discussion

3.1. Characterization of catalysts

The surface morphology of Fe_3S_4, GO and GO-Fe_3S_4 were investigated with SEM as shown in Fig. 2. Fe_3S_4 exhibited a structure of microsphere with many uniform pores, having particle size ranged from 2 to 8 μm (Fig. 2a and b). GO distinctly exhibited a sheet structure and its flakes were consisted of few-layered curly nanosheets (Fig. 2c). The GO-Fe_3S_4 composite had a hybrid morphology of nanosheets and nanoparticles: the assembling Fe_3S_4 nanoparticles on GO sheets result in a multilayer plate-like structure (Fig. 2d), and the nanoparticles on the surface of the plates have particle sizes of 20–40 nm, which was much smaller than that of Fe_3S_4 microspheres (Fig. 2a and b). This makes clear that the introduction of GO in the preparation course of Fe_3S_4 particles was contribute to the crystallization of Fe_3S_4 particles with minor sizes. Except that, it could also found that the dispersion of GO nanosheets becomes somewhat worse after combination with Fe_3S_4 (as showed in Fig. 2d). This may due to the formation of hydrogen bonds between the hydroxyl groups from ethylene glycol and GO during the preparation of the composite. As GO dispersing in the aqueous solution of ethylene glycol, they may attract each other, which induce the slight intercalated agglomeration of GO. The similar phenomenon was also found in other reports(Suter et al., 2020). However, this trivial agglomeration has little effect on the specific surface area of the composite, which was further confirmed by the next BET results.

Fig. 3a, b and c showed the nitrogen sorption isotherms of Fe_3S_4, GO and GO-Fe_3S_4 at 77 K. The BET analysis showed that the specific surface area of GO-Fe_3S_4 composite was 7.71 m²/g, which was much larger than that of Fe_3S_4 (1.94 m²/g). The specific surface area of GO prepared in this work was 306.02 m²/g. The prominent enhanced BET area of this composite indicated that GO was a superior carrier to the fixation of Fe_3S_4 nanoparticles. The pore-size distribution of the samples was estimated by employing the Barreet–Juyner–Halenda (BJH) method, which was showed in the inset of Fig. 3a, b and c. By comparison with Fe_3S_4, the GO-Fe_3S_4 composite have more *meso*-pores at 18.9, 34.3, 37.1 and 40.0 nm, which resulted in its larger specific surface area.

The XRD spectrum of Fe_3S_4, GO and GO-Fe_3S_4 were showed in Fig. 3d. It was found that the characteristic peaks ((0 0 1) and (1 0 1)) of GO are located at 11.20° and 42.24°, respectively, which are basically consistent with the standard characteristic peak of GO. The major characteristic peaks of Fe_3S_4 ((3 1 1), (2 2 2), (4 0 0), (5 1 1) and (4 4 0)) are located at 30.12°, 32.95°, 36.48°, 52.67° and 54.77°, respectively. In addition, other weak diffraction peaks ((1 1 1), (2 2 0), (4 2 2), (5 3 1), (6 2 0) and (4 4 4)) were located at 18.04°, 25.64°, 47.27°, 59.54°, 61.37°, 64.13° and 68.74°, respectively. GO-Fe_3S_4 composite had the similar characteristic peaks as Fe_3S_4, but with higher peak intensity and crystallinity. Except that, the characteristic peaks of GO ((0 0 1) and (1 0 1)) were also existed in the XRD pattern of the composite. This indicated that Fe_3S_4 nanoparticles were well loaded on the surface of GO. The crystallite sizes of Fe_3S_4 and GO-Fe_3S_4 composite were determined by

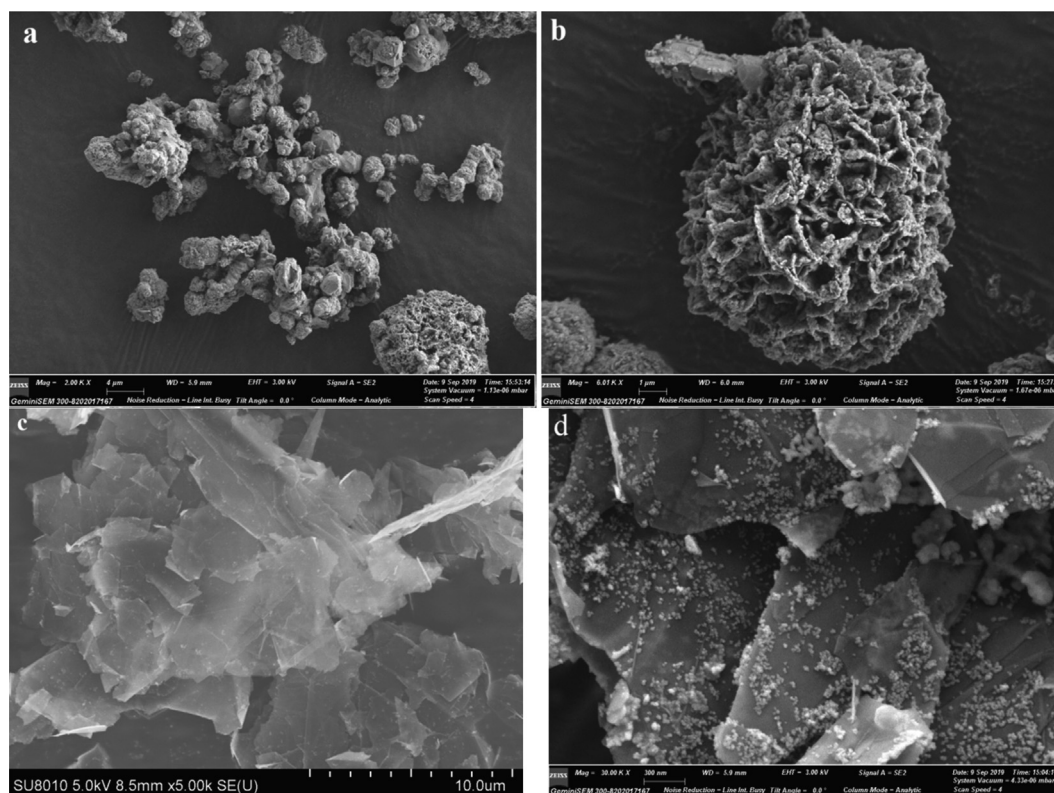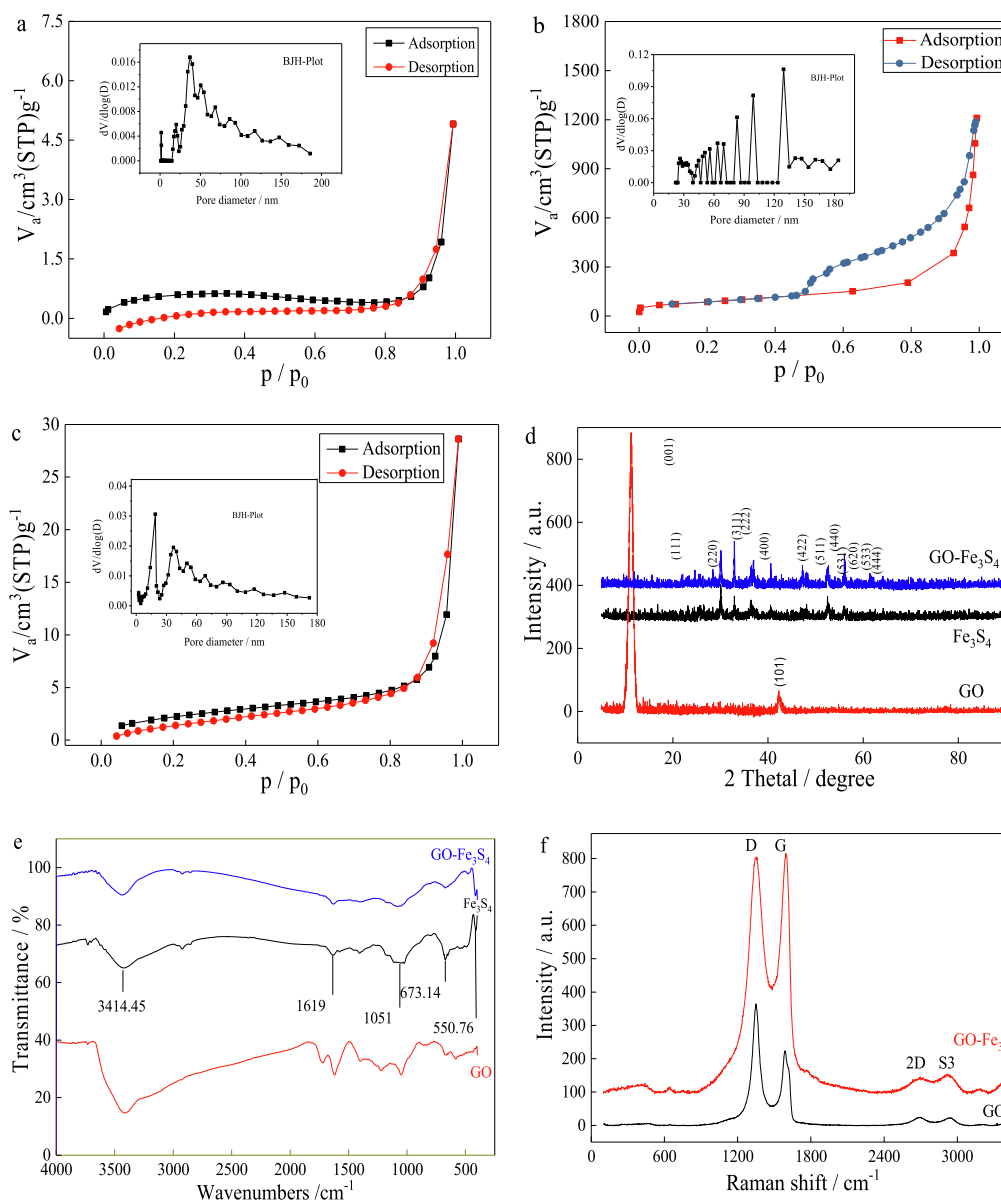**Fig. 2** SEM analysis of different catalysts (a、b) Fe_3S_4, (c) GO and (d) GO-Fe_3S_4.

Fig. 3 Nitrogen sorption isotherms for (a) Fe_3S_4, (b) GO and (c) GO-Fe_3S_4. The inset showed the corresponding pore-size distribution. (d) XRD patterns of Fe_3S_4, GO and GO-Fe_3S_4 composite. (e) FT-IR spectra of GO, Fe_3S_4 and GO-Fe_3S_4 composite. (f) Raman spectra of Fe_3S_4 and GO-Fe_3S_4 composite.

employing Scherrer equation $(d = k\lambda/(\beta\cos\theta))$, which gave the crystallites sizes of 26.11 nm and 29.63 nm, respectively.

The FT-IR spectrum of GO, Fe_3S_4 and GO-Fe_3S_4 were displayed in Fig. 3e. The absorption peaks of GO at 3414, 1727 and 1619 cm^{-1} may be due to the vibration of –OH, stretching vibration of –COOH, and the asymmetric and symmetrical stretching vibration of C=O, respectively. The absorption peaks of Fe_3S_4 at 3425, 1631, 1406 and 1025 cm^{-1} may be corresponding to the stretching vibration of O—H, bending vibration of O—H, stretching vibration of C—C and stretching vibration of C—C or C—O. Almost all the adsorption peaks of GO and Fe_3S_4 were existed in the spectrum of GO-Fe_3S_4 composite, indicating that Fe_3S_4 nanoparticles were distributed on the surface of GO.
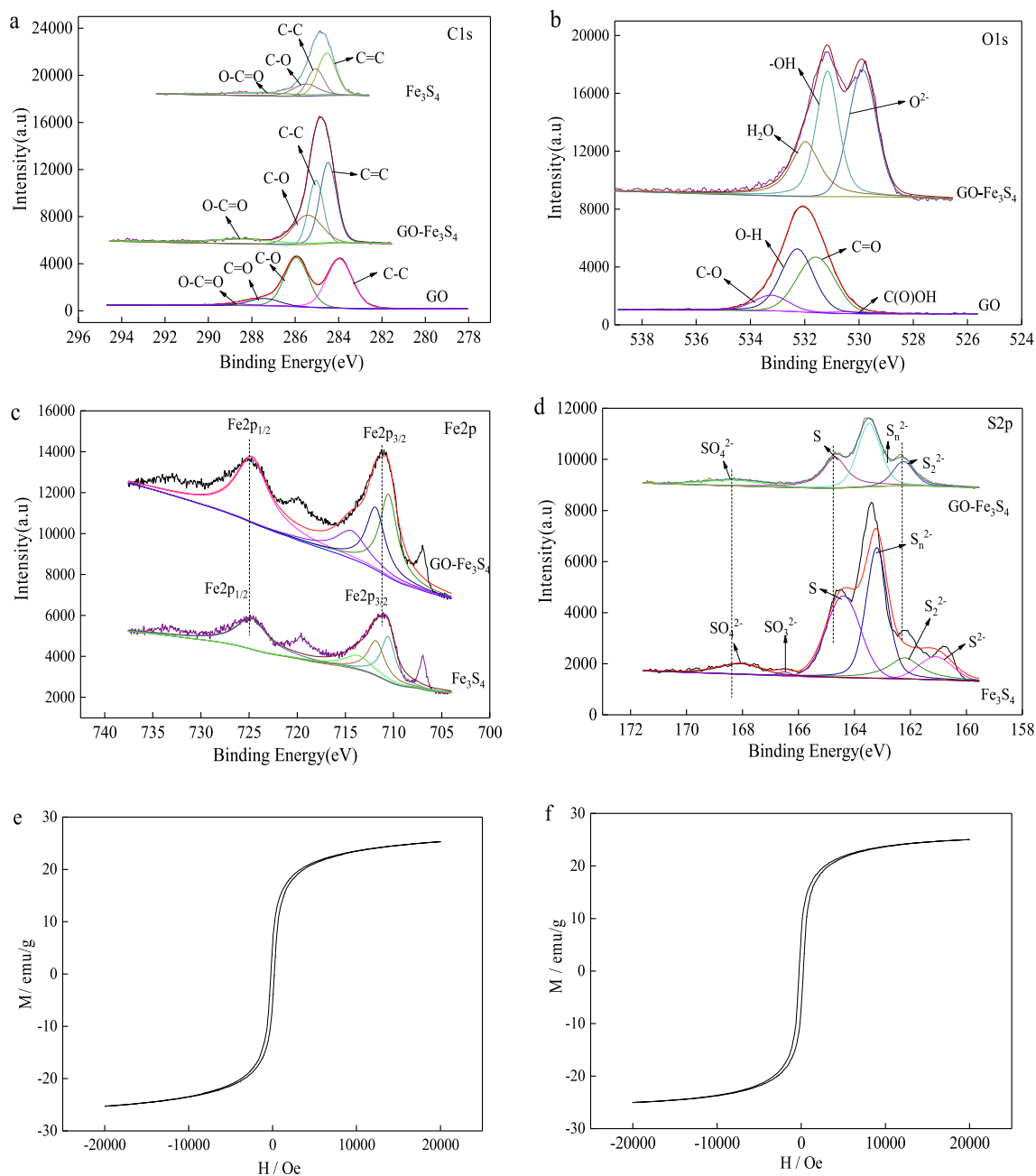
The Raman spectra of GO and GO-Fe_3S_4 were compared in Fig. 3f. In the Raman spectra of GO, the G (corresponding to the first-order scattering of the E_{2g} mode) and D bands (as a breathing mode of κ-point phonons of A_{1g} symmetry) (A.C. Ferrari and J. Robertson 2000) were seen at 1588 cm^{-1} and 1348 cm^{-1}, respectively. After loading Fe_3S_4 on the surface of GO, the G and D bands were shifted to 1593 and 1352 cm^{-1}, respectively. And the corresponding intensities of the two bands were obviously increasing. It was likewise observed that the peak intensity ratio of I_D/I_G was decreased from 1.63 to 0.98, indicating an increase in the mean size of the sp^2 domains after the hydrothermal treatment. It may attribute to the introducing of the oxygen-containing groups, such as –OH, during the process of hydrothermal treatment. Otherwise, the 2D peak around 2680 cm^{-1} resulting from the second order of zone-boundary phonons (Ferrari et al., 2006) and the S3 peak near 2930 cm^{-1} rooting in the lattice disorders referring to the combination of the G and D bands (Tung et al.,

2009, Cuong et al., 2010) were also found in the Raman spectra of GO and GO-Fe$_3$S$_4$. As reported in previous studies, the shape and location of 2D peak are concerned with the formation and the layer number of GO (I. Calizo et al., 2007, , Cooper et al., 2020). The 2D peak location of single-layer graphene sheets was observed at 2679 cm^{-1} and its location transferred to higher frequencies by 19 cm^{-1} with the multilayer increasing from 2 to 4 (Graf, et al., 2007). In the Raman spectrum of GO-Fe$_3$S$_4$ composite, the 2D peak was detected at about 2695 cm^{-1}, showing the formation of 2 to 4-layers GO sheets.

XPS analysis was conducted to explored chemical composition of GO-Fe$_3$S$_4$ composite and to analyze the interaction between GO and Fe$_3$S$_4$. The C1s, O1s, Fe2p and S2p envelops of GO, Fe$_3$S$_4$ and GO-Fe$_3$S$_4$ composite were displayed in Fig. 4a-d and their deconvolution was carried out via employing a Gaussian-Lorentzian peak shape after conducting a Shirley background correction. The C1s peak in the spectrum of Fe$_3$S$_4$ was very weak, which was assigned to the residual carbon in the organic reagents (such as ethylene glycol) after the solvothermal process during Fe$_3$S$_4$ preparation, yet the much enhanced C1s signals in the spectrum of GO-Fe$_3$S$_4$ composite ascribed to the introduction of GO. The C1s deconvolution of the GO-Fe$_3$S$_4$ composite associated with the existence of the C—O, O-C=O and C—C bonding at binding energies of 285.4, 288.4 and 285.05 eV, respectively. The O1s envelops

Fig. 4 XPS spectra for GO, Fe$_3$S$_4$ and GO-Fe$_3$S$_4$ composite. (a) C1s envelop, (b) O1s envelop, (c) Fe2p envelops and (d) S2p envelop. Magnetic properties (M−H curve) of (e) Fe$_3$S$_4$ and (f) GO-Fe$_3$S$_4$ composite.

of GO and GO-Fe$_3$S$_4$ composite were compared as shown in Fig. 4b. It was observed that O in GO samples mainly exists in the form of C—O, O—H, C═O, and C(O)OH. The O in GO-Fe$_3$S$_4$ samples was primary in the form of O^{2-} groups (OH$^-$, SO$_3^{2-}$ and SO$_4^{2-}$) and H$_2$O. The corresponding binding energy of O in GO-Fe$_3$S$_4$ was lower than that in GO. The Fe2p XPS spectra of Fe$_3$S$_4$ and GO-Fe$_3$S$_4$ composite was displayed in Fig. 4c. No remarkable difference was found in Fe2p XPS spectra of Fe$_3$S$_4$ and GO-Fe$_3$S$_4$. The S2p spectra of Fe$_3$S$_4$ and GO-Fe$_3$S$_4$ were also compared (Fig. 4d). It was found that S element in Fe$_3$S$_4$ exists in multiple valence states, including SO$_3^{2-}$, SO$_4^{2-}$ and S-Fe at binding energies of 166.5, 168.1 and 164.59 eV, respectively. By comparison with Fe$_3$S$_4$, the elemental binding energy of S-Fe and S—O in GO-Fe$_3$S$_4$ was shifted from 164.59 and 168.1 to 164.69 and 168.37 eV, respectively. The change of elemental binding energy (the chemical shift) ascribe to the distinction in the chemical potential and polarizability of S ion. Therefore, it is speculated that the C—S—C bond is formed in the time of the composite preparation.

The M−H curve of Fe$_3$S$_4$ certified that its saturation magnetization. The saturation moment per unit mass (Ms) was approximately 25.30 emu g^{-1} (Fig. 4e), which was agreed well with previous report (Zhang and Chen 2009). The saturation magnetization of GO-Fe$_3$S$_4$ composite was 25.03 emu g^{-1} (Fig. 4f), indicating that the introduction of GO have no remarkable effect on the magnetic property of Fe$_3$S$_4$. The superparamagnetic property of GO-Fe$_3$S$_4$ composite makes it easy to separate from the wastewater and reutilize fatherly.

3.2. Heterogeneous Fenton like catalytic degradation of water-soluble lignin model compounds by GO-Fe$_3$S$_4$ composite

3.2.1. Degradation of vanillic acid in various systems
Considering the chemical structure of water-soluble lignin, vanillic acid and PHBA were selected as model compounds. Fig. 5a compared the degradation of vanillic acid in different reactive systems. The vanillic acid was observed to undergo little degradation in the systems of Fe$_3$S$_4$-pollutant and GO-Fe$_3$S$_4$-pollutant. However, the degradation of vanillic acid was greatly enhanced by the introduction of oxidizing agent (H$_2$O$_2$). Compared to the reactive systems containing Fe$_3$S$_4$ as the catalyst, the presence of H$_2$O$_2$ in the GO-Fe$_3$S$_4$ system showed a much faster degradation rate of vanillic acid. About 94 % of vanillic acid was removed in 15 min in the GO-Fe$_3$S$_4$-H$_2$O$_2$-pollutant system. The degradation of vanillic acid probably followed a pseudo first order reaction in kinetics ($\ln(c_0/c) = kt$). By fitting $\ln(c_0/c)$ as a function of the reaction time t, linear relationships were obtained as shown in Fig. 5b. The apparent rate constant was increased with an addition of GO and H$_2$O$_2$ into the reaction system. The apparent rate constant is in the order of Fe$_3$S$_4$-pollutant (1.14×10^{-4} min^{-1}) < GO-Fe$_3$S$_4$-pollutant (1.31×10^{-3} min^{-1}) < Fe$_3$S$_4$-H$_2$O$_2$-pollutant (6.22×10^{-2} min^{-1}) < GO-Fe$_3$S$_4$-H$_2$O$_2$-pollutant (1.81×10^{-1} min^{-1}). Therefore, GO-Fe$_3$S$_4$ composite is an effective heterogeneous Fenton-like catalyst for the degradation of vanillic acid. In Fenton reaction, the dosage of H$_2$O$_2$ as a major oxidant plays an important part (Vilar et al., 2009, Rocha et al., 2011). The concentration of H$_2$O$_2$ in various systems with the absence of vanillic acid was monitored (Fig. 5d). It was found that the decomposition rate of H$_2$O$_2$

was 78 % and 66 % after 90 min in the systems of GO-Fe$_3$S$_4$-H$_2$O$_2$-pollutant (curve 2 in Fig. 5d) and Fe$_3$S$_4$-H$_2$O$_2$-pollutant (curve 1 in Fig. 5d), respectively. The kinetics of H$_2$O$_2$ decomposition in the aforesaid systems followed a pseudo first order reaction (Fig. 5e). The H$_2$O$_2$ decomposition rate, k, in GO-Fe$_3$S$_4$-H$_2$O$_2$-pollutant system is 1.42×10^{-2}, which was higher than that ($k = 8.90 \times 10^{-3}$) in Fe$_3$S$_4$-H$_2$O$_2$-pollutant system. The hydroxyl radicals generated in the systems were also monitored (Fig. 5f). The generation of •OH radicals in various systems likewise abided by the identical sequence as H$_2$O$_2$ decomposition. In consequence, it can be concluded that the GO-Fe$_3$S$_4$ composite owns stronger catalysis ability than Fe$_3$S$_4$.

### 3.2.2. Effects of catalyst preparation condition
By studying the degradation of vanillic acid in the GO-Fe$_3$S$_4$-H$_2$O$_2$ system, the influence of catalyst preparation parameters on the heterogeneous Fenton-like catalytic performance of the composite were explored. Fig. S1a and Fig. 6a showed the effect of catalyst preparation temperature on the degradation rate constant of vanillic acid. Below 180 °C, the degradation rate of vanillic acid was increased with the enhancement of temperature. This may ascribe the enhanced crystallinity of this composite at a high temperature. With the increasing of calcination temperature (over 180 °C), the degradation constant was decreased with increased temperature, which may be related to the destruction of the crystalline structure of the composite at temperatures higher than 180 °C. Therefore, the optimal preparation temperature was selected as 180 °C.

The GO content in the composite likewise affects the degradation of vanillic acid (Fig. S1b and Fig. 6b). It was observed that the degradation rate of vanillic acid was firstly increased with the increased content of GO, reaching the maximum value, and then decreased promptly. The optimal GO content was 4 %. When the GO content was below 4 %, increasing the GO content, means more and more Fe$_3$S$_4$ nanoparticles dispersed on the surface of GO, avoiding the agglomeration of the catalyst particles and enhancing the contact area of catalyst, oxidizing agent and pollutants. Thus the adsorption and catalytic performance of the composite were improved, resulting in the high degradation efficiency of the pollutant. When the GO content was higher than 4 %, the dispersion of Fe$_3$S$_4$ nanoparticles on GO surface was enough. While superabundant GO could not activated H$_2$O$_2$ which reduce the producing of high oxidizing active species. Therefore, the optimal GO content was 4 %.

3.2.3. Effects of catalyst load and H$_2$O$_2$ concentration
In addition to the preparation condition of the composite, the reaction conditions in the catalytic system were also important influence factors to the degradation of vanillic acid. With the increasing of catalyst load, the degradation rate of vanillic acid was firstly increased and then declined after reaching a maximum value (Fig. S1c and Fig. 6c). The maximum degradation rate constant of vanillic acid was 0.181 min^{-1} with catalyst load of 0.4 g/L. The concentration of H$_2$O$_2$ has a similar effect on the degradation of vanillic acid: k value was primarily enhanced with the enhancement of H$_2$O$_2$ concentration and then declined as its concentrations beyond 12 mmol/L (Fig. 6d and Fig. S1d). This may probably be related to that the superfluous of H$_2$O$_2$ can lead to the scavenging effect of
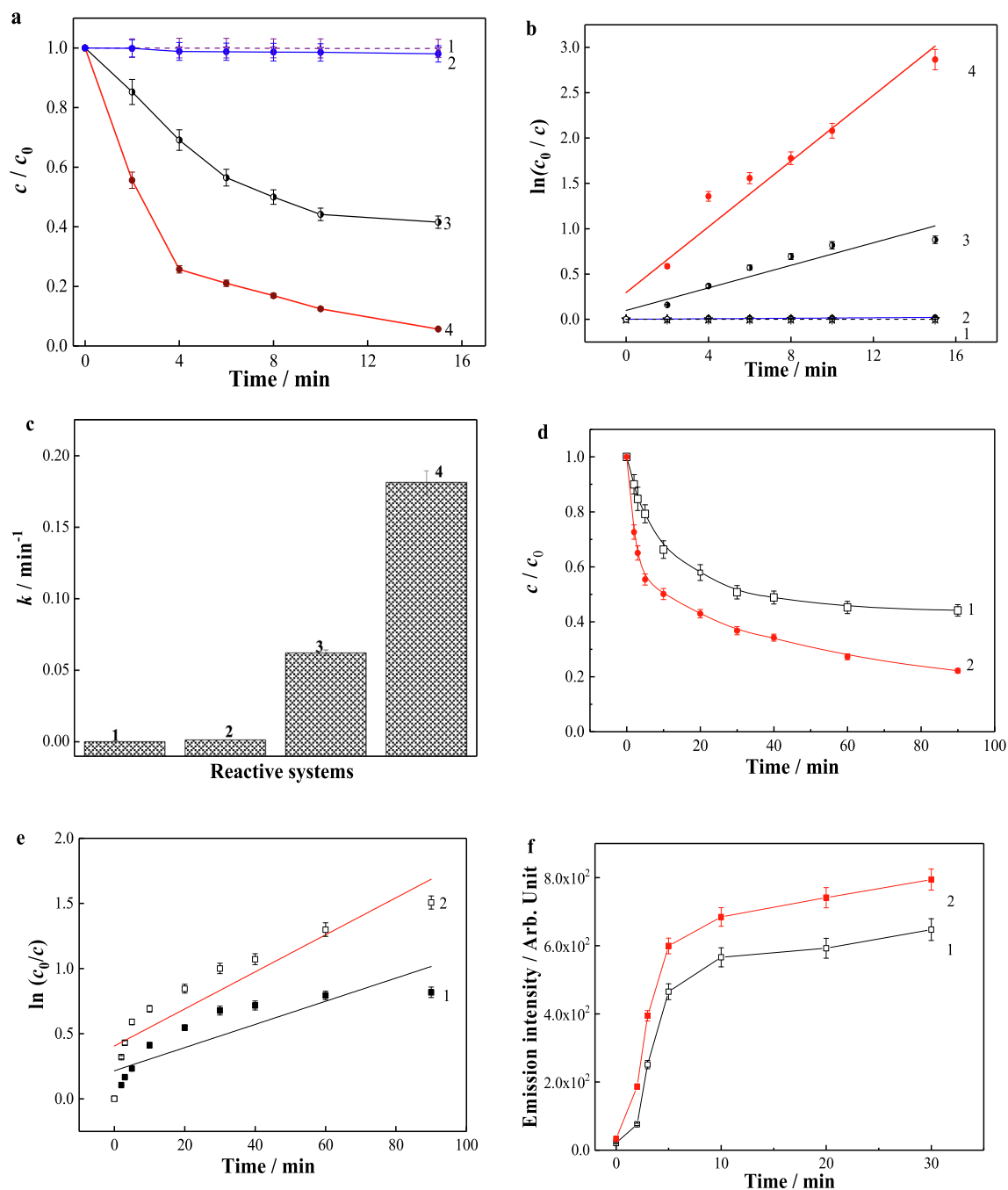
Fig. 5 (a) Degradation of vanillic acid and (b) its kinetics and (c) rate constants in different systems of (1) Fe_3S_4-pollutant, (2) GO-Fe_3S_4-pollutant, (3) Fe_3S_4-H_2O_2-pollutant and (4) GO-Fe_3S_4-H_2O_2-pollutant. Reaction time dependences of (d, e) the H_2O_2 consumption and (f) the fluorescence intensity in the systems of (1) Fe_3S_4-H_2O_2 and (2) GO-Fe_3S_4-H_2O_2 (without vanillic acid). Reaction conditions: catalyst load 0.4 g/L, vanillic acid concentration 35 mg/L, solution pH 4, and initial H_2O_2 concentration 12 mmol/L.

$\bullet$OH radicals. Hence, the optimal concentration of H_2O_2 was 12 mmol/L.

3.2.4. Effects of initial solution pH and reactive temperature

Initial solution pH affects the adsorption of vanillic acid on GO-Fe_3S_4 composite and the degradation of the substrate (Fig. S1e). Fig. 6e showed that the degradation rate constant of vanillic acid was enhanced with the increasing of pH value from 2 to 4. The degradation of vanillic acid was influenced by

the adsorption of vanillic acid on the catalyst. This is primary due to the charges on the surface of the catalyst. The adsorption of vanillic acid on composite was firstly increased as pH value was increased from 2 to 4, reaching the maximum value, and then decreased while pH greater than 4 (Fig. 6e). By monitoring the zeta potential of GO-Fe_3S_4 composite at various pH value (Fig. S2), it was observed that the composite carried positive charges at the pH range of 2–6. The positive charges were decreased with increasing pH value. Vanillic acid has a
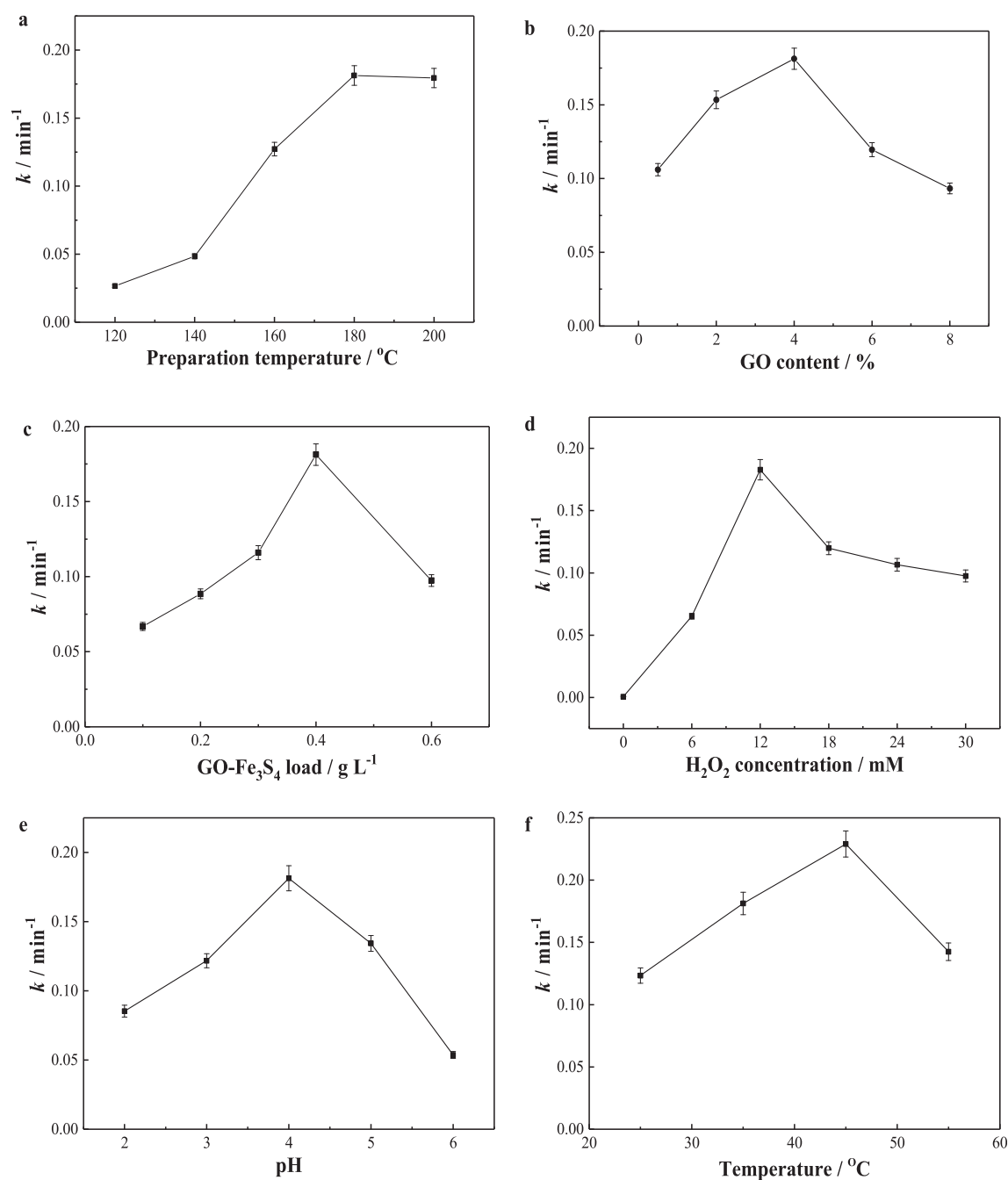
Fig. 6 Effects of (a) preparation temperature and (b) GO content of GO-Fe$_3$S$_4$ composite on the rate constant of vanillic acid degradation. The GO content was 4 % in (a), and the preparation temperature of the composite was 180 °C in (b). Dependence of vanillic acid degradation rate constant on (c) catalyst load, (d) initial H$_2$O$_2$ concentration, (e) solution pH value and (f) reactive temperature for GO-Fe$_3$S$_4$ composite. Other reaction conditions: vanillic acid concentration 35 mg/L, GO-Fe$_3$S$_4$ composite load 0.4 g/L(a, b, d, e, f), initial H$_2$O$_2$ concentration 12 mmol/L(a, b, c, e, f), solution pH 4 (a, b, c, d, f), and reactive temperature 35 °C (a, b, c, d, e).

pK$_a$ value of 4.53. When the pH was increased from 2 to 4, vanillic acid was gradually dissociated and existed in the form of negative ions. Therefore, the electrostatic attraction between GO-Fe$_3$S$_4$ composites and vanillic acid become stronger, enhancing the adsorption of vanillic acid to the composite. The better adsorption always induces a higher catalytic effect and degradation efficiency. When the pH value was above 4, the positive charges of GO-Fe$_3$S$_4$ composites were continuously decreased. Meanwhile, the vanillic acid was almost com-

pletely dissociated. These reduce the electrostatic attraction between GO-Fe$_3$S$_4$ composites and vanillic acid, weakening the adsorption of the pollutants to the composite (Fig. S3). Furthermore, the inherent H$_2$O$_2$-activation ability of Fe$_3$S$_4$ was declined with increasing pH in the range of 4–6. Hence, the catalytic activity of the GO-Fe$_3$S$_4$ composite was reduced further with the increasing of pH value from 4 to 6. It ought to be pointed out that the solution pH value may affect the particle sizes and further impact the catalytic performance of

catalysts. Nevertheless, it was found in our study that the hydromechanic particle size of GO-Fe$_3$S$_4$ composite was changed slightly from 2588 to 3742 nm with the enhancement of pH value from 2 to 6. As a result, the influence of solution pH value to the adsorption and degradation performance of vanillic acid was not caused by the hydromechanic particle size of GO-Fe$_3$S$_4$ composite.

Reaction temperature plays important roles in the heterogeneous Fenton like process. It was observed that the degradation k value of vanillic acid was firstly increased from 1.23×10^{-1} to 2.29×10^{-1} min^{-1} with the enhancement of temperature from 25 °C to 45 °C. This may due to the fact that the high temperature accelerated the mass transfer efficiency in the reactive system, which increased the contact chance between reactive oxygen species and pollutants. As the temperature increased further, H$_2$O$_2$ may be decomposed into O$_2$ and H$_2$O, reducing the generation of highly reactive species. As a consequence, the degradation rate constant was reduced. Considering temperature effect as well as the energy cost, the optimal reaction temperature could be 35 °C.

3.2.5. Optimization of the vanillic acid degradation over GO-Fe$_3$S$_4$ composite

For purpose of farther optimizing the vanillic acid degradation conditions in system of GO-Fe$_3$S$_4$-H$_2$O$_2$, the response surface methodology (RSM) based on the central composite design (CCD) was employed to assess and optimize the effect of the independent variables (GO-Fe$_3$S$_4$ load, H$_2$O$_2$ concentration and initial pH value) on the response variable (degradation efficiency of vanillic acid). The three independent variables were transformed into dimensionless (A, B, C), which was respectively studied at five levels (–alpha, low, center, high and + alpha coding as 1.68, −1, 0, +1, +1.68, respectively). On account of our elementary experiments, the selected values of the variables were showed in Table 2. The experimental and predicted values of vanillic acid degradation efficiency under different reaction conditions gained from RSM-CCD were listed in Table 3. It was found that the predicted degradation rates of vanillic acid generated from this model were in accord with the experimental dates. And it could be farther proved by plotting the predicted degradation rate versus experimental dates (Fig. 7), in which the slope about the line of the best fit was 0.9966 and R^2 was observed to be 0.9967. The suitable model equation incorporated 10 statistically significant coefficients was obtained according to coded factors and displayed in Eq. (1) as follows:

$$D = 92.92 + 11.89A + 8.14B - 4.35C - 4.56AB$$
$$- 2.82AC - 1.56BC - 16.53A^2 - 17.11B^2 - 18.32C^2 \quad (1)$$

Where, D represents the degradation rate of vanillic acid. And A, B and C is on behalf of the corresponding independent variables. And the positive and negative coefficients exhibited the active and passive effect to the degradation efficiency of vanillic acid (Hazime et al., 2013).

In addition to correlation coefficients, the discrepancy between laboratory and predicted dates (residuals) could likewise be employed to assessing the conformity of this model (Chen et al., 2012). As shown in Fig. S4, all residuals were good accord with the line which made clear that no distinct non-normality was found. Furthermore, it displayed in Fig. S5 that the residuals were stochastically distributed around zero with a variation of ± 3.15. From the above results, it could be revealed that the acquired model is employable to reveal the relation between the independent variables and vanillic acid degradation rate. The analysis of variance was exhibited in Table S1. It could be found that the model was remarkable for vanillic acid degradation thanks to the F-value of 331.34 and p-value below 0.0001. The coefficients and adjusted coefficients of vanillic acid degradation were 0.9967 and 0.9936, respectively, indicating that the response of this model was well consistent to the experimental dates (Wang et al., 2018). The co-efficient of variance of vanillic acid degradation rate was 3.80, displaying a high precision and good reliability of this model (Sulaiman et al., 2019).

Moreover, the two-dimensional contour plots and three dimensional surface plots were carried out to explore the individual and combined influence of independent variables on vanillic acid degradation. It was observed that all two-dimensional contour plots displayed elliptical contour, indicating that the interplay between independent variables were prominent (Song et al., 2020). It was found in Fig. 8(a) that the degradation rate of vanillic acid was improved with the enhancement of GO-Fe$_3$S$_4$ load and H$_2$O$_2$ concentration (solution pH value: 4) until it reached the maximum value. As the GO-Fe$_3$S$_4$ load and H$_2$O$_2$ concentration are exceeded their optimum value, the degradation efficiency of vanillic acid was declined due to the unfavorable consumption of active radicals. Fig. 8b showed the combined effects of GO-Fe$_3$S$_4$ loads and solution pH in the time of H$_2$O$_2$ concentration was kept at 12 mM. As proved, the degradation rate of vanillic acid was increased with the enhancement of solution pH value and GO-Fe$_3$S$_4$ loads. The maximum degradation efficiency was observed in a solution around pH = 4. The effect of H$_2$O$_2$ concentration and solution pH, in which the GO-Fe$_3$S$_4$ load was fixed at 0.4 g/L, on vanillic acid degradation was displayed in three dimensional surface and two-dimensional contour plot (Fig. 8c). It was observed that the degradation rate of vanillic acid reached the maximum value of 94.3 % at 12 mM of H$_2$O$_2$ and pH 4. The solution pH value had no remarkable

Table 2 Experimental range and levels of the independent variables for the degradation of vanillic acid.

Independent variables	Coded levels				
	-alpha (-1.68179)	Low (-1)	Center(0)	High(1) (+1)	+ alpha (+1.68179)
GO-Fe$_3$S$_4$ (g/L): A	0.06	0.2	0.4	0.6	0.7
H$_2$O$_2$(mM): B	1.9	6	12	18	22. 1
Solution pH: C	0.6	2	4	6	7.4

Table 3 Experimental data of CCD.

Run	Independent variables			Degradation Rate (%)	
	A	B	C	Experimental	Predicted
1	0.7	12	4	68.24	66.18
2	0.4	12	7.4	35.87	33.77
3	0.6	6	2	54.36	54.89
4	0.4	22.1	4	61.35	58.22
5	0.6	6	6	42.41	43.67
6	0.4	1.9	4	31.52	30.85
7	0.06	12	4	27.92	26.19
8	0.4	12	4	94.31	92.92
9	0.4	12	4	92.45	92.92
10	0.2	6	2	15.39	16.34
11	0.4	12	0.6	50.12	48.42
12	0.2	18	6	36.53	38.68
13	0.6	18	2	63.04	65.17
14	0.4	12	4	93.24	92.92
15	0.4	12	4	91.58	92.92
16	0.2	6	6	15.85	16.41
17	0.6	18	6	45.96	47.69
18	0.4	12	4	93.46	92.92
19	0.4	12	4	91.84	92.92
20	0.2	18	2	43.45	44.88
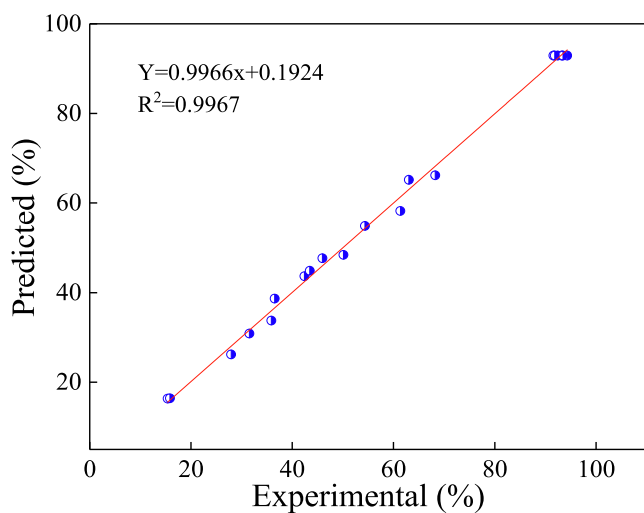
Fig. 7 Correlation of predicted and experimental values of response for vanillic acid degradation.

$Y = 0.9966x + 0.1924$
$R^2 = 0.9967$

Table 4 Intermediate products of vanillic acid degradation.

Serial number	material	m/z	Molecular formula
1	vanillic acid	168.15	$C_8H_8O_4$
2	2-methoxy-1,4-dihydroxyphenol	140	$C_7H_8O_3$
3	hydroxyquinone	124	$C_6H_4O_3$
4	1,2,4-dihydroxyphenol	126	$C_6H_6O_3$
5	3-hydroxyglutaric acid	148	$C_5H_7O_5$
6	3, 4-Dihydroxybutyric acid	120	$C_4H_7O_4$
7	malonic acid	104	$C_3H_4O_4$
8	malic acid	134	$C_4H_6O_5$
9	propylene glycol	120	$C_3H_4O_5$
10	guaiacol	124	$C_7H_8O_2$
11	Catechol	110	$C_6H_6O_2$
12	cis,cis-muconic acid	142	$C_6H_6O_4$
13	Maleic acid	116	$C_4H_4O_4$
14	glycolic acid	76	$C_2H_4O_3$
15	oxalic acid	90	$C_2H_2O_4$

influence on the vanillic acid degradation and the optimal pH was at the scope of 3.0–5.0 at the optimal H_2O_2 concentration and GO-Fe_3S_4 load. Hence, it could be deduced that the solution pH value was the least impact factor attribute to the lower F value (54.40), followed by H_2O_2 concentration (190.08) and GO-Fe_3S_4 loads (405.66) (Table S1). According to the model, the degradation rate of vanillic acid was able to achieve the maximum value (92.92 %) at the optimal reactive conditions (GO-Fe_3S_4 load: 0.4 g/L, H_2O_2 concentration: 12 mM and solution pH value: 4) with the desirability of 0.954. Three additional experiments at the optimal conditions were conducted to verify the predictive ability of the model. It was found that the degradation rates of vanillic acid in above experiments were

92.5 %, 91.6 % and 93.5 %, respectively, which manifested that the model had a good predictive ability under the optimal reactive conditions.

The adsorption is important to the degradation efficiency in heterogeneous Fenton like reaction. Strong adsorption affinity of pollutants on catalysts increases the reaction probability of pollutants with the active spices, enhancing the degradation of pollutants. The adsorption of vanillic acid on Fe_3S_4, GO-Fe_3S_4 composite and the mixture of Fe_3S_4 and GO were studied under the optimized conditions. As shown in Fig. 9a, the adsorption capacity of vanillic acid on Fe_3S_4, GO-Fe_3S_4 composite and the mixture of Fe_3S_4 and GO were 2.437, 21.87 and

(a)

(b)

(c)
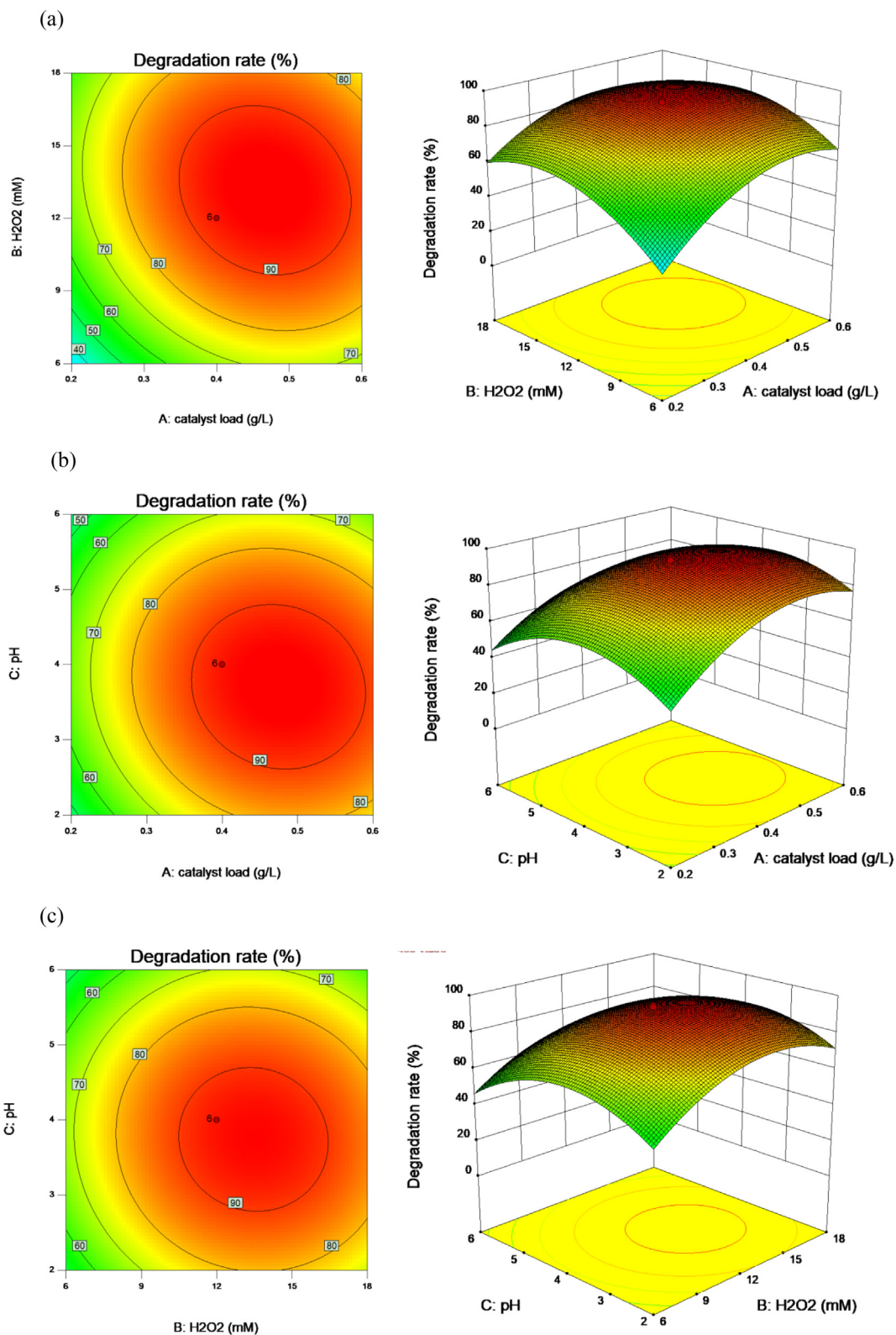
Fig. 8 2D contour plots and 3D surface plots of vanillic acid degradation over GO-Fe$_3$S$_4$ catalyst as a function of (a) catalyst loads and H$_2$O$_2$ concentrations, (b) catalyst loads and solution pH and (c) H$_2$O$_2$ concentrations and solution pH.

2.971 mg g^{-1}, respectively. The composite showed a higher adsorption affinity and this is due to its larger surface area measured by BET (7.71 m^2/g for GO-Fe$_3$S$_4$ composite and 1.94 m^2/g for Fe$_3$S$_4$). It can be concluded that the larger surface area of the composite strengthened its adsorption performance, resulting in a stronger catalytic ability. Except for the
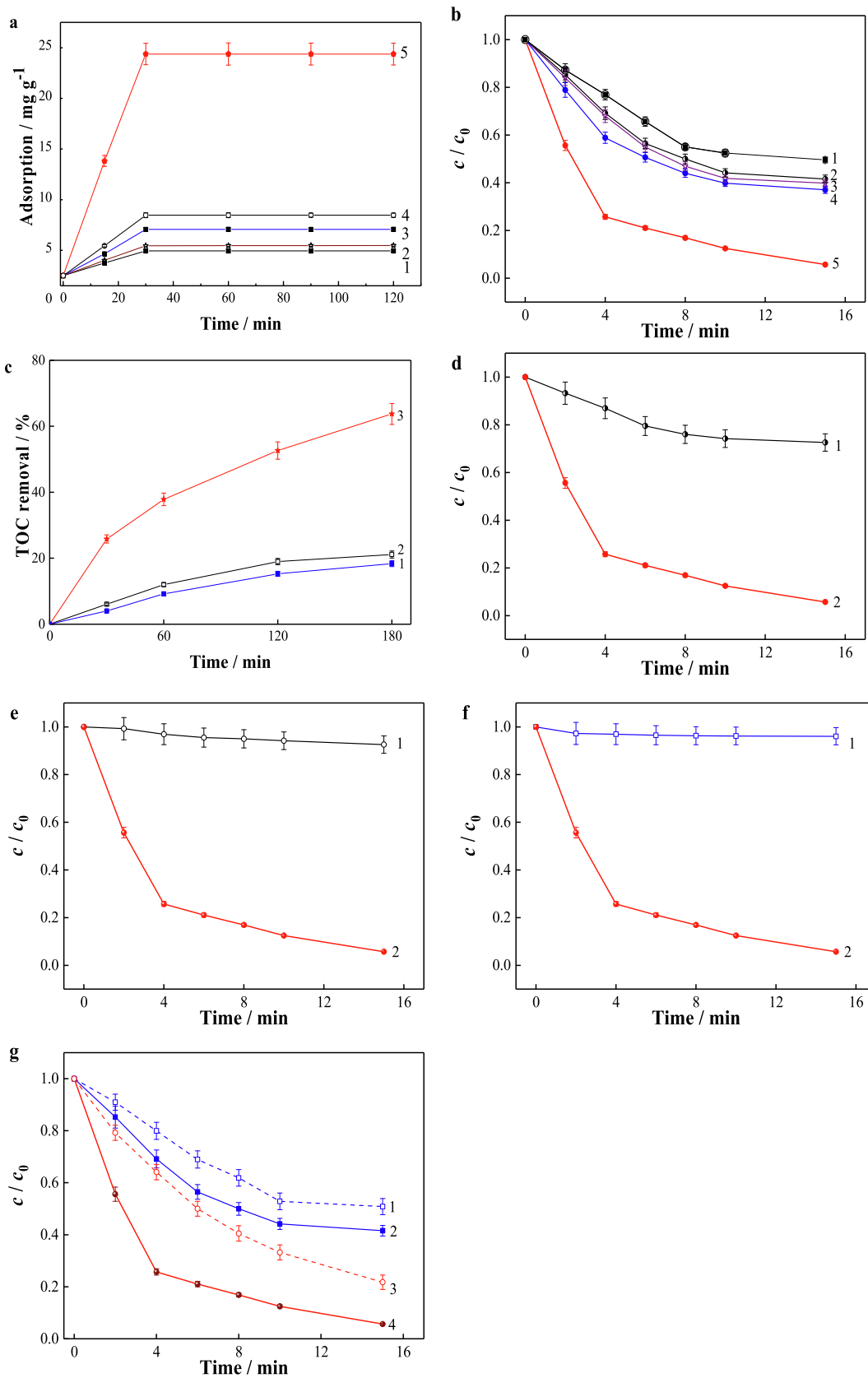
surface area, the hydrogen-bonding interaction and π-π stacking effect between GO and vanillic acid may also improve the adsorption between them. The adsorption performance of vanillic acid to the GO-Fe₃S₄ composite was compared to other two high-efficient catalysts, including graphene-BiFeO₃ composite and biochar-CuFeO₂ (Hazime et al., 2013, Xin et al., 2021). As shown in Fig. 9a, the adsorption of vanillic acid on GO-Fe₃S₄ composite was stronger than the other two catalysts.

The degradation of vanillic acid by employing different catalysts under the optimal conditions was also compared in Fig. 9b. Compare to Fe₃S₄, the mechanical mixing of GO and Fe₃S₄ increased the degradation rate constant from 6.22×10^{-2} to 6.56×10^{-2} min^{-1}. While, the GO-Fe₃S₄ composite showed degradation rate constant of 1.81×10^{-1} min^{-1}, which was 2.91 or 2.76 folds to Fe₃S₄ or the mixture of Fe₃S₄ and GO, respectively. The decomposition of H₂O₂ and generation of •HO was much more effective by the catalysis of GO-Fe₃S₄ composite. About 95 % of vanillic acid was removed in 15 min. The catalytic ability of GO-Fe₃S₄ composite was further evaluated by comparing the degradation of vanillic acid under the same conditions which was catalyzed by the above composite, graphene-BiFeO₃ composite and biochar-CuFeO₂, respectively. As shown in Fig. 9b, the degradation of vanillic acid by the GO-Fe₃S₄ composite was remarkably rapid than those by the other two catalysts. Hence, the GO-Fe₃S₄ composite was an excellent heterogeneous Fenton catalyst.

The removal of total organic carbon (TOC) in different systems catalyzed by various catalysts was investigated (Fig. 9c). It was found that about 63.8 % of TOC was removed in 180 min from the GO-Fe₃S₄-H₂O₂-vanillic acid system. However, the removal of TOC was only 18.4 % and 21.1 % which was catalyzed by Fe₃S₄ and the mixture of GO and Fe₃S₄, respectively. Therefore, the GO-Fe₃S₄ composite could remove TOC efficiently in the reaction system.
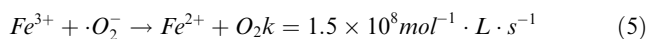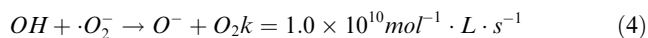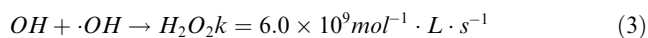
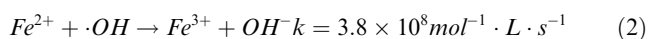### 3.2.6. Catalytic mechanism analysis

The active species generated from the reactive system of GO-Fe₃S₄-H₂O₂ were explored. The major active species causing the degradation of the substrate was proposed to be •OH radicals. This was confirmed preliminarily by the next study. As we know, isopropyl alcohol could quench •OH radicals. And it was introduced to the GO-Fe₃S₄-H₂O₂ system. It was observed that the degradation efficiency of vanillic acid was restrained obviously in comparison with the system without the isopropyl alcohol (Fig. 9d). The degradation rate constant in GO-Fe₃S₄-H₂O₂ system was 1.81×10^{-1} min^{-1}, while it was reduced dramatically to

2.25×10^{-2} min^{-1} with the adding of isopropyl alcohol. The contribution rate of •OH radical was estimated on the basis of the formula of $Contribution rate = \left(1 - \frac{k_q}{k}\right) \times 100\%$ (k_q and k represents the degradation constant rate of vanillic acid with or without isopropyl alcohol, respectively). It was obtained that the contribution rate of hydroxyl radical was 87.6 %. Considering the hydroxyl radicals generated from the composite may existed on the surface on the catalyst and in bulk solution. The contributions of surface-bound hydroxyl radicals and free hydroxyl radicals to vanillic acid degradation were evaluated. It has been found that surface-bound hydroxyl radicals could be desorbed from the catalyst surface by adding superfluous KI because of the formation of •OH…I⁻ (Martin et al., 1995). Therefore, the degradation of vanillic acid was investigated with adding KI. It was observed in Fig. 9e that the degradation of vanillic acid was almost completely restricted by the introduction of KI, which indicated that the Fenton activity of GO-Fe₃S₄ was dominated by the surface-bound hydroxyl radicals. In view of iron ions may dissolve from the composite to the bulk solution during the heterogeneous Fenton process, the degradation of vanillic acid was investigated in corresponding homogeneous Fenton system. The homogeneous Fenton process was carried out as follows: GO-Fe₃S₄ was firstly dispersed in deionized water and stirring for 120 min, followed by filtering the solid catalyst from solution. And then vanillic acid was added to above solution. The homogeneous Fenton reaction was started by the adding of H₂O₂. Fig. 9f exhibited that the degradation of vanillic acid in the above homogeneous Fenton system was little (no more 4 % of pollutant was removed), which manifested that heterogeneous Fenton process governed the degradation of vanillic acid. Therefore, it can be concluded that the vanillic acid degradation in the GO-Fe₃S₄-H₂O₂ reactive system was dominated by surface reaction. And the hydroxyl radicals bounded on the compound surface was the main oxygen species in reactive system.

As mentioned above, the oxidizing agent in above reactive system was hydrogen peroxide. Except H₂O₂, other species such as molecular oxygen may also be activated in Fenton process. The molecular oxygen could be activate to generate •O₂⁻ by a single-electron transfer process as Eqs. (1), which was able to promote the iron redox cycle in Fenton process. And the abundant reductive sites on the surface of Fe₃S₄ was capable of activating molecular oxygen to produce •O₂⁻ (Shi et al., 2020). The contribution of •O₂⁻ to the degradation of vanillic acid was compared between Fe₃S₄-H₂O₂ and GO-Fe₃S₄-H₂O₂ reactive system by adding SOD (•O₂⁻ scavenger) to the

Fig. 9 (a) Adsorption and (b) degradation of vanillic acid over different catalysts. Catalysts: (1) Fe₃S₄, (2) the mixture of GO and Fe₃S₄, (3) Biochar-CuFeO₂, (4) graphene-BiFeO₃ and (5) GO-Fe₃S₄. (c) TOC removal during the vanillic acid degradation over different catalysts. Catalysts: (1) Fe₃S₄, (2) the mixture of GO and Fe₃S₄ and (3) GO-Fe₃S₄. (d) Degradation kinetics of vanillic acid catalyzed by GO-Fe₃S₄ composite with (1) or without (2) the introduction of isopropyl alcohol. (e) Degradation kinetics of vanillic acid catalyzed by GO-Fe₃S₄ composite with (1) or without (2) the introduction of KI. (f) Degradation kinetics of vanillic acid catalyzed by GO-Fe₃S₄ composite in dissolved iron ion-H₂O₂ system (1) and GO-Fe₃S₄-H₂O₂ system (2). (g) Degradation kinetics of vanillic acid in different systems (1: Fe₃S₄-H₂O₂-SOD; 2: Fe₃S₄-H₂O₂; 3: GO-Fe₃S₄-H₂O₂-SOD; 4: GO-Fe₃S₄-H₂O₂). Adsorption and degradation conditions: vanillic acid concentration 35 mg/L (a-g), catalyst load 0.4 g/L (a-g), initial H₂O₂ concentration 12 mmol/L (b-g), solution pH 4 (a-g), and reactive temperature 35 °C (a-g).

two systems. It was observed in Fig. 9g that the addition of SOD both inhibited the degradation of vanillic acid in the two systems, which demonstrated that $\bullet O_2^-$ could be favor the degradation of the pollutant. However, the contribution of $\bullet O_2^-$ in the two systems was different. And the contribution rate of $\bullet O_2^-$ was primary evaluated as follows: $Contribution rate = \frac{k-k_{sod}}{k} \times 100\%$, which k_{sod} and k represent the degradation rate constant of vanillic acid with or without SOD addition, respectively. The contribution rate of $\bullet O_2^-$ to vanillic degradation was evaluated as 21 % and 40 % in systems of Fe_3S_4-H_2O_2 and GO-Fe_3S_4-H_2O_2, respectively. The larger contribution rate in GO-Fe_3S_4-H_2O_2 system compared with that of Fe_3S_4-H_2O_2 system may be ascribed to the much reductive sites on the surface of GO-Fe_3S_4. The reason may be described as follows: firstly, GO-Fe_3S_4 composite possessed larger specific surface than that of Fe_3S_4, which exposed much more reductive sites on the surface of catalysts. Secondly, the stronger adsorptive performance of GO-Fe_3S_4 composite to vanillic acid was able to accumulate the pollutants on the surface of the composite effectively. Thus the generated oxygen species in this reactive system would be consumed rapidly in a short time, avoiding the over-oxidation of reductive site on the surface of the catalyst. As a result, the abundant reductive sites on the surface of GO-Fe_3S_4 composite were able to activate molecular oxygen to generate $\bullet O_2^-$ efficiently, promoting the iron redox cycle of the GO-Fe_3S_4 Fenton system. Therefore, ferrous ions was produced more effectively, resulting in the high conversion rate of H_2O_2 to $\bullet OH$ (Eqs. (2)-(5)).

$$Fe^{2+} + O_2 \rightarrow Fe^{3+} + \cdot O_2^- \tag{1}$$

$$Fe^{2+} + \cdot OH \rightarrow Fe^{3+} + OH^- \quad k = 3.8 \times 10^8 mol^{-1} \cdot L \cdot s^{-1} \tag{2}$$

$$OH + \cdot OH \rightarrow H_2O_2 \quad k = 6.0 \times 10^9 mol^{-1} \cdot L \cdot s^{-1} \tag{3}$$

$$OH + \cdot O_2^- \rightarrow O^- + O_2 \quad k = 1.0 \times 10^{10} mol^{-1} \cdot L \cdot s^{-1} \tag{4}$$

$$Fe^{3+} + \cdot O_2^- \rightarrow Fe^{2+} + O_2 \quad k = 1.5 \times 10^8 mol^{-1} \cdot L \cdot s^{-1} \tag{5}$$

3.3. Degradation intermediates and a possible reaction mechanism

The degradation intermediates of vanillic acid were explored with LC-MS compared with authentic reference standards (Fig. S6). In addition to the parent vanillic acid (**1**), fourteen intermediates (**2–15**) were recognized (Table 4). On account of the identified intermediates, tentative degradation pathways of vanillic acid were concluded (Fig. 10).

The degradation of vanillic acid in GO-Fe_3S_4-H_2O_2 system was triggered through two possible pathways. The first one (labeled as I) was that a carbonyl group was removed from vanillic acid (**1**), producing intermediate **2**, which was subsequently demethylated and dehydrogenated to form intermediate **4**. Except that, intermediate **2** could also be directly demethoxy to generate intermediate **4**. Subsequently, the benzene ring in intermediate **4** was broken down by the oxidizing active species, which caused the generation of intermediate **5** following the decarbonization and hydroxylation. Intermediate **5** was then transformed into intermediate **6** via decarboxylation. And intermediate **6** was farther oxidized to intermediate **7**, which was subsequently oxidized to intermediate **8**. Then it

was further oxidized to form intermediate **9**. Intermediate **9** was then transformed into intermediate **15** via decarbonization. And it may further be oxidized to CO_2 and H_2O. The second one (labeled as II) was that vanillic acid was directly decarboxylated to form intermediate **10**. And it was further transformed into intermediate **11** through demethoxylation. Intermediate **11** was oxidized through ring-opening reaction to form intermediate **12** which was further oxidized to form intermediate **13** via decarboxylation. Intermediate **13** was oxidized to intermediate **14** and was farther hydroxylated to form intermediate **15**. Finally, it may be mineralized into CO_2 and H_2O.

The degradation of PHBA in GO-Fe_3S_4-H_2O_2 system was also studied. Under optimal conditions (catalyst load: 1 g/L, H_2O_2 concentration: 18 mmol/L, pH 4, temperature: 35 °C), 99.79 % of p-hydroxybenzoic acid (25 mg/L) was degraded in 15 min. The degradation intermediates of PHBA were also identified with LC-MS compared with authentic reference standards (Fig. S7). Fifteen intermediates (**2–16**) from the degradation of PHBA (**1**) were identified. Based on the identified intermediates, tentative degradation pathways of p-hydroxybenzoic acid were proposed (Fig. 11). There are two possible pathways for the degradation of PHBA. The first one (labeled as I) was that PHBA (**1**) was transformed to intermediate **2** by hydroxylation following the forming of intermediate **3** through hydroxylation reaction. Intermediate **3** was decarboxylated to form intermediate **4**, in which the benzene ring was broken down by oxidation reaction to form intermediate **5** through decarbonization and hydroxylation. Subsequently, intermediate **5** was transformed to intermediate **6** through decarboxylic reaction. Intermediate 6 was then oxidized to intermediate **7**, **8** and **13**. Intermediate **13** was converted to intermediate **14** through decarboxylation and decarbonization. Intermediate **14** was oxidized to intermediate **15** and subsequently converted to intermediate **16** by hydroxylation. In addition, PHBA could also be directly converted to intermediate **9** by decarboxylation (labeled as II). And intermediate **9** was then converted to intermediate **10** through hydroxylation. Subsequently, intermediate **10** was oxidized to form intermediate **11** through ring-opening reaction and hydroxylation. Intermediate **11** was broken down through decarbonization to form intermediate **12** which was then converted to intermediate **13** through hydroxylation. Intermediate **13** was subsequently oxidized to intermediate **14**, **15** and **16**. And intermediate **16** may be oxidized to CO_2 and H_2O.

According to the study of the degradation pathways of the above two compounds, it was found that the degradation process included the hydroxylation, ring-opening reaction, decarboxylation and decarbonization. Finally, the compounds were broken down to carboxylic acids with low molecular weight.

In order to further investigate the degradation process of vanillic acid and PHBA, the accumulation and elimination of intermediates of the above compounds was analyzed by detecting the change of peak area of corresponding intermediates (Fig. 12). It was observed that the parent compounds were degraded rapidly which corresponding peak area was decreased promptly in first 30 min. And the concentration of selected intermediates (intermediates **5**, **12** and **15** for vanillic acid in Fig. 12a; intermediates **5**, **11** and **16** for PHBA in Fig. 12b) were firstly increased, reached the maximal value and then decreased sharply, which indicated that the oxidative active species were attack the intermediates continuously and
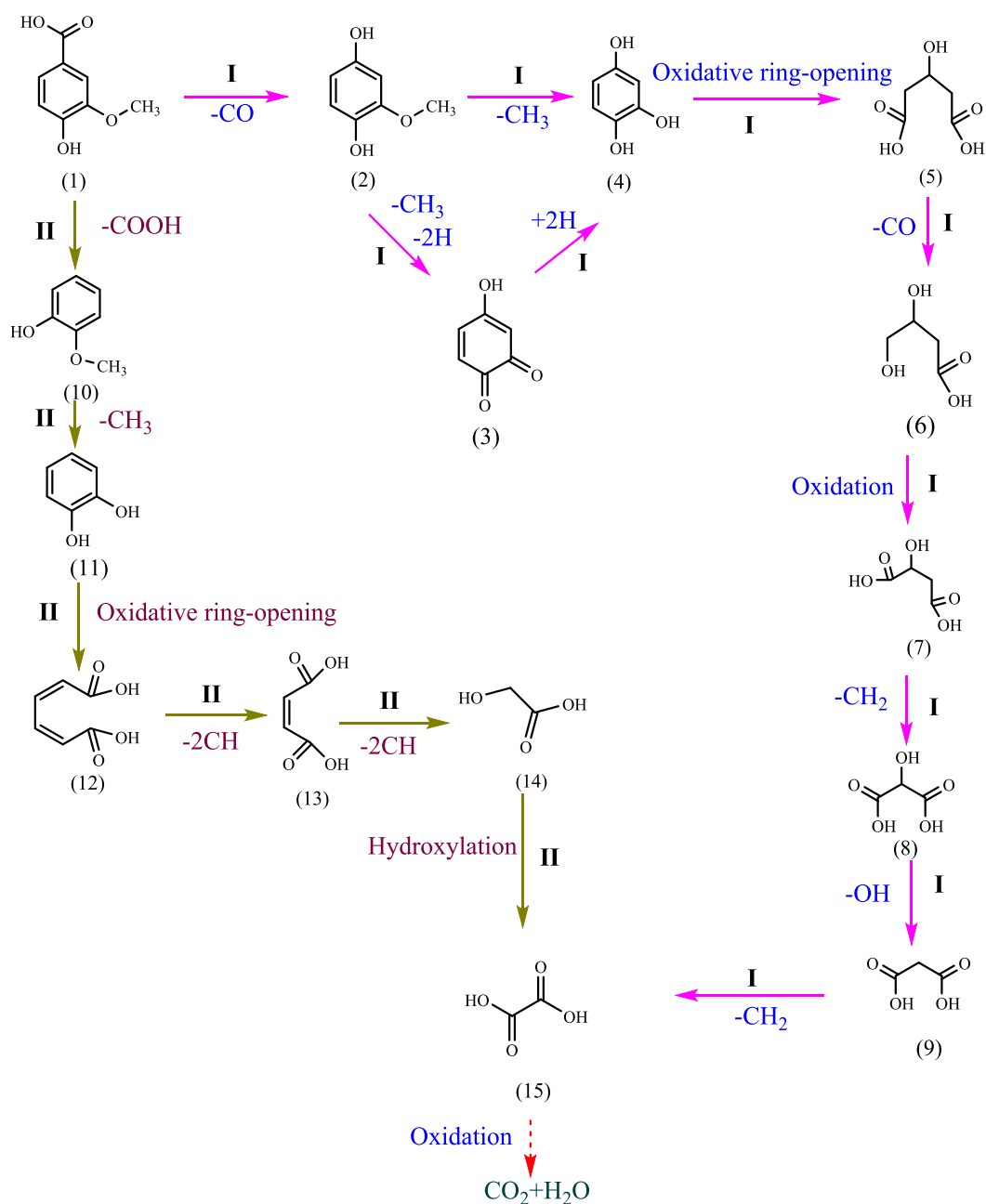
Fig. 10 Proposed pathways for vanillic acid degradation in the system of GO-Fe$_3$S$_4$-H$_2$O$_2$.

resulting the high degradation efficiency of them. This further conformed that the GO-Fe$_3$S$_4$-H$_2$O$_2$ system could effectively degrade and mineralize organic pollutants.

3.4. The practical application of GO-Fe$_3$S$_4$-H$_2$O$_2$ system for the disposal of wastewater discharged from papermaking mills

To further evaluate the application value of GO-Fe$_3$S$_4$-H$_2$O$_2$ system for the degradation of pollutants in wastewater, the above system was applied to dispose the effluent discharged from the secondary biochemical process in pulping and papermaking mills (COD: 160 ∼ 200 mg/L ; chromaticity: 200). The COD and chromaticity removal efficiency of secondary biochemical effluent in GO-Fe$_3$S$_4$-H$_2$O$_2$ system were compared

with homogeneous Fenton process (Fe^{2+}/S$_2$O$_8^{2-}$–H$_2$O$_2$ system) which was utilized widely in practical. And the concentration of oxidizing agent in the two systems was almost equal. It was observed in Fig. 13 that the COD removal efficiency in Fe^{2+}/S$_2$O$_8^{2-}$–H$_2$O$_2$ system was increased rapidly in first 40 min. And then the removal efficiency was slowly increased with the next time. The maximal COD removal efficiency was 66 %. This may because the generation rate of hydroxyl radicals and sulfate radicals was declined at the later stage of reaction. Except that, the long distance between radicals to pollutants in bulk water body reduced the mass transfer efficiency which also exhibited the degradation of pollutants. Compared with the above homogeneous Fenton process, the COD removal efficiency in GO-Fe$_3$S$_4$-H$_2$O$_2$ system was much
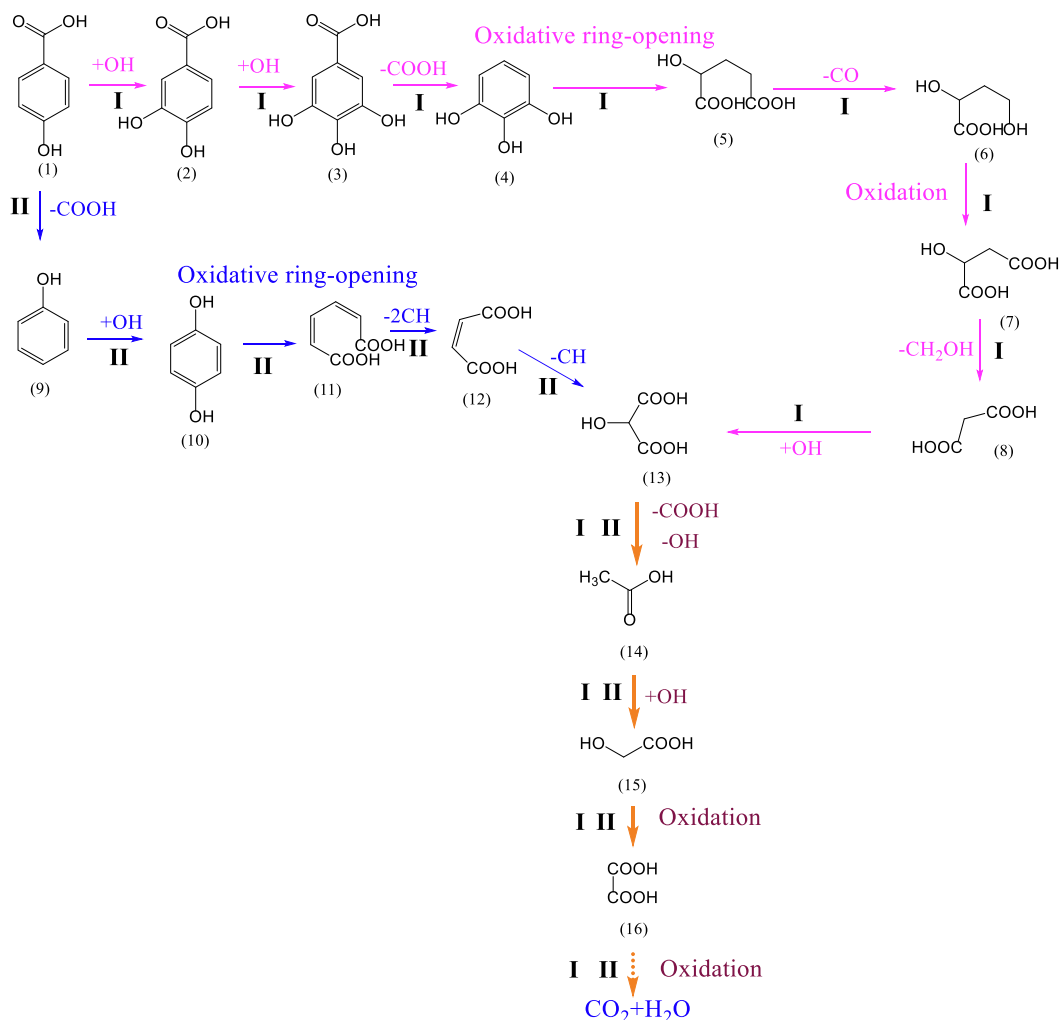
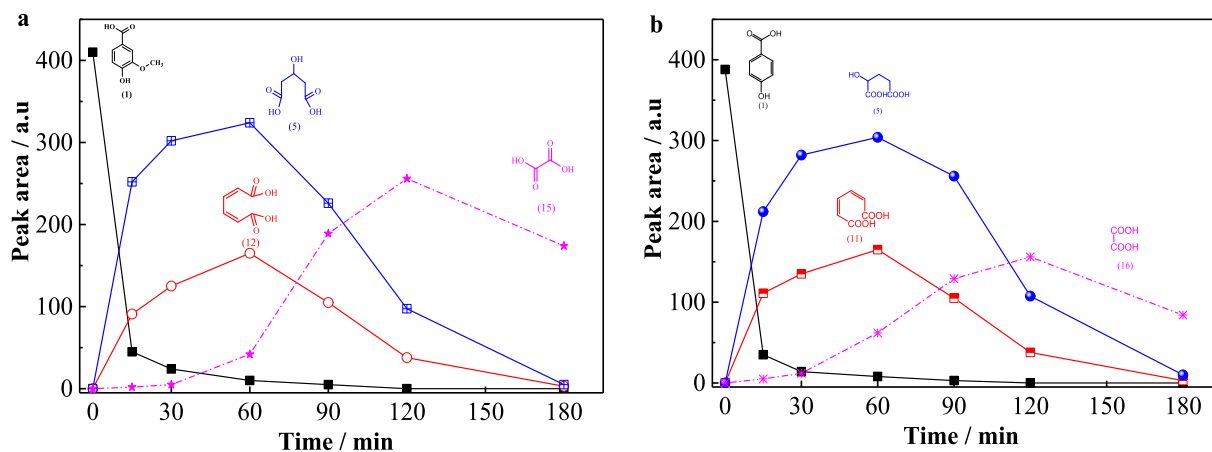**Fig. 11**   possible path of PHBA degradation.

Fig. 12   The change of peak area of parent and intermediates during the degradation of vanillic acid (a) and PHBA (b).

higher. The optimal COD removal efficiency was increased to 95 %. The degradation in heterogeneous Fenton process was mainly happened on the surface of the catalyst. The adsorption of pollutants to catalyst surface shortens the distance from active radicals to pollutants, which enhanced the mass trans-

form efficiency in reactive system. Thus the degradation of pollutants was increased. The chromaticity removal efficiency in the above two systems were also compared. As shown in Fig. 13, the chromaticity removal efficiency in $Fe^{2+}/S_2O_8^{2-}$–H_2O_2 system was increased to 66 % in first 80 min, and then
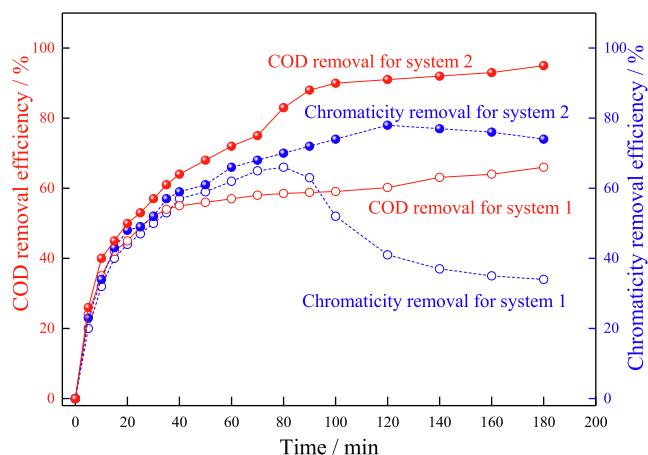
Fig. 13 The removal efficiency of COD and chromaticity of secondary biochemical effluent in different systems (system 1: $Fe^{2+}/S_2O_8^{2-}$–H_2O_2 system; system 2: $GO-Fe_3S_4$-H_2O_2). Degradation conditions: system 1: Fe^{2+} concentration: 2.25 mmol/L, $S_2O_8^{2-}$ concentration: 1.05 mmol/L, H_2O_2 concentration: 0.45 mmol/L, solution pH 3, reactive temperature 25 °C; system 2: catalyst load 0.05 g/L, initial H_2O_2 concentration: 1.5 mmol/L, solution pH 4 and reactive temperature 25 °C.

decreased in the next time. This may induce to the oxidation reaction of Fe^{2+} to Fe^{3+}, which generated the yellow color in wastewater. While the chromaticity removal in $GO-Fe_3S_4$-H_2O_2 system was more efficient (about 78 % of chromaticity was removed). And the chromaticity removal efficiency was almost not declined after reached the maximal value. This further confirmed that the dissolution of iron ions from $GO-Fe_3S_4$ was little which induce tiny effect to the color of the wastewater. The higher removal efficiency of COD and chromaticity in $GO-Fe_3S_4$-H_2O_2 system compared with homogeneous Fenton process indicated that the system possessed large potential application value in practice.

### 3.5. Stability and reusability of GO-Fe₃S₄ composite

The stability and reusability of $GO-Fe_3S_4$ composite was estimated. And the recycling experiment of the composite was firstly carried as follows: the catalyst was first gathered by

using a magnet, after the added vanillic acid was almost completely degraded. Next, the supernatant was centrifuged to collect the residual catalyst in it. After the two parts of the catalysts were made together, it was suspended into a fresh solution of vanillic acid and H_2O_2, and the vanillic acid was continued as the second cycle. This process was repeated several times. It was observed from recycling experiment results that the composite were able to be reutilized for first five cycles without the remarkable damage of catalytic activity (Fig. S8). The degradation rate constant of the vanillic acid was 1.81×10^{-1}, 1.76×10^{-1}, 1.72×10^{-1}, 1.69×10^{-1} and 1.69×10^{-1} min^{-1} for the first five cycles. After reused five times, the catalytic activity of $GO-Fe_3S_4$ composite could maintain 93 %, which preliminarily confirmed the good stability and reusability of the composite. Furthermore, no dissolving of S ions from $GO-Fe_3S_4$ composite was monitored during the reuse of $GO-Fe_3S_4$ composite for the vanillic acid degradation at pH 4.0 by atomic absorption spectrometry, and the leaching of Fe ions was no more than ca. 1 % (Fig. S9). The negligible dissolving of S and Fe ions further confirmed that the composite was relatively stable in the catalytic system. Therefore, it can be concluded that the composite was stable and could be reutilized without the loss of catalytic activity.

3.6. Contributions of GO to the catalytic activity of GO-Fe₃S₄ composite

GO sheets play an importation role in the $GO-Fe_3S_4$ composite, which has three functions in the heterogeneous Fenton like catalyst. The first is that the introducing of GO can make Fe_3S_4 particles disperse well in the catalyst, resulting in the grain sizes of $GO-Fe_3S_4$ composite of 20–40 nm, being much smaller than that of Fe_3S_4 (2–8 μm). The second is that GO sheets can promote the adsorption performance of $GO-Fe_3S_4$ composite. Due to the smaller particle size and porous structure, the specific surface area was enhanced from 1.94 m^2/g (Fe_3S_4) to 7.71 m^2/g ($GO-Fe_3S_4$). Especially, the oxygen-containing groups on the surface of GO sheets were favorable to the dispersion of catalyst particles in the aqueous phase. These hydrophilic groups can efficiently adsorb the water-soluble pollutants from water (such as water-soluble lignin compounds) by the formation of chemical bond (such as hydrogen bonds). Except that, because of the large π bonds
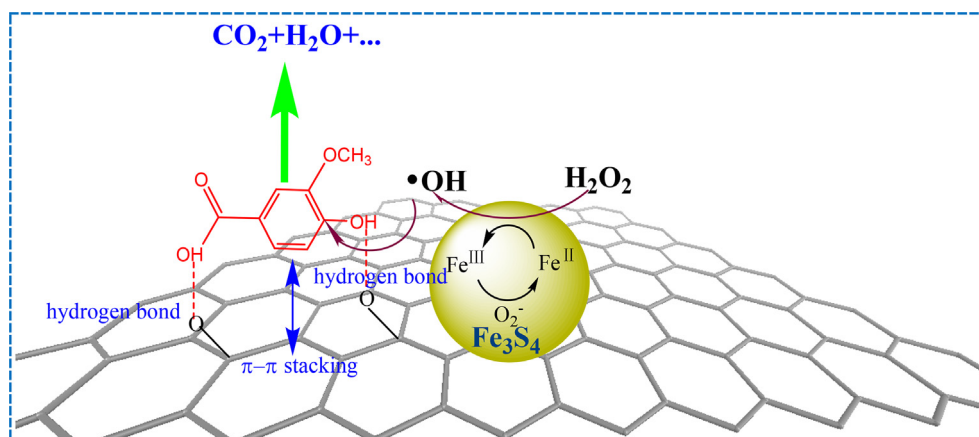
Fig. 14 the adsorptive and catalytic mechanism of $GO-Fe_3S_4$ composite.

existed in GO, the benzene ring in lignin molecules can easily linked to the surface of graphene oxide by the π-π stacking (Fig.S10 showed the FT-IR spectra of GO-Fe$_3$S$_4$, vanillic acid and GO-Fe$_3$S$_4$ adsorbed by vanillic acid, indicating that the composite can effectively adsorb vanillic acid under the experiment condition). The third one is the most important and is related to the high mass transfer efficiency of oxidizing radicals in reaction system. This resulted in high catalytic efficiency by increasing the contact time between the reactive oxygen species and pollutants. Because of the short life of reactive species (for example: •OH < 1 μs), the distance between reactive species and pollutant molecules has a very significant effect on the degradation efficiency of pollutants. The introduction of GO could accumulate the pollutants in the bulk solution to the surface of the composite, which shorten the distance between pollutants and catalysts. Thus, the reactive oxidizing species could directly attack the molecules of pollutants, improving the degradation efficiency of pollutants. As previously discussed, the rapidly consume of oxygen species avoided the overoxidation of reductive sites on the surface of the composite, which promoted the generation of •O$_2^-$. Thus, the conversion of H$_2$O$_2$ to •OH was further enhanced. The adsorptive and catalytic mechanism of GO-Fe$_3$S$_4$ composite was shown in Fig. 14.

4. Conclusions

A GO-Fe$_3$S$_4$ nanoscaled composite based on the matrix of GO sheet has been synthesized by using the solvothermal method and investigated as a Fenton-like catalyst. Through the BET analysis, it was found that the specific surface area of GO-Fe$_3$S$_4$ composite was 7.71 m^2/g, which was larger than that of Fe$_3$S$_4$ (1.94 m^2/g). And the composite could adsorb water-soluble lignin model pollutants more effectively with the π-π stacking effect and the formation of hydrogen bonds between catalyst and substrate, which induced high mass transfer efficiency of oxidizing radicals in reactive system. Hence, the GO-Fe$_3$S$_4$ composite possessed remarkable heterogeneous Fenton-like catalytic performance toward the degradation of vanillic acid and PHBA. It was discovered that the catalytic ability of this composite was affected by its preparation condition and reactive parameters in catalytic system. Through the preliminary optimization of preparation and reaction conditions, the degradation rate constant of vanillic acid by using the GO-Fe$_3$S$_4$ composite as catalyst could achieve 1.81×10^{-1} min^{-1}, being 2.91 or 2.76 folds of that gained by Fe$_3$S$_4$ or the mixture of Fe$_3$S$_4$ and GO, respectively. RSM was conducted to farther optimize the vanillic acid degradation condition. And the suitable model equation was obtained. The catalytic mechanism in GO-Fe$_3$S$_4$-H$_2$O$_2$ system was analyzed fatherly. The degradation of pollutants was dominated by surface reaction. And the main oxidizing species was the hydroxyl radicals bounded on the surface of the composite. Except H$_2$O$_2$, molecular oxygen in the system could also be activated to generate •O$_2^-$ by the reductive sites on the surface of GO-Fe$_3$S$_4$, which promoted the conversion of H$_2$O$_2$ to •OH. The analysis of degradation intermediates of vanillic acid and PHBA showed that the pollutants were degraded to smaller molecules by oxidation reactions. The analysis of degradation intermediates concentration of the vanillic acid and PHBA showed that the pollutants were degraded and mineralized efficiently. The comparison of GO-Fe$_3$S$_4$-H$_2$O$_2$ system to other homogeneous Fenton process in the application of disposing effluents generated from the secondary biochemical process in pulping and papermaking mills further confirmed that the reactive system possessed potential application prospect in practical. Excellent heterogeneous Fenton catalytic performance of GO-Fe$_3$S$_4$ composite were ascribed to its larger surface area, plenty of reductive active sites and efficient mass transfer of oxidizing radicals in the reactive system.

References

An, J., Zhu, L., Wang, N., et al, 2013. Photo-Fenton like degradation of tetrabromobisphenol A with graphene-BiFeO$_3$ composite as a catalyst. Chem. Eng. J. 219, 225–237. https://doi.org/10.1016/j.cej.2013.01.013.

H. Bader, V. Sturzenegger and J. Hoigne, 1988. Photometric method for the determination of low concentrations of hydrogen peroxide by the peroxidase catalyzed oxidation of N,N-diethyl-p-phenylene-diamine (DPD). Water Res. https://doi.org/https://doi.org/10.1016/0043-1354(88)90005-X

Bentivenga, G., C. Bonini, , M. D'Auria, , et al., 2003. Degradation of steam-exploded lignin from beech by using Fenton's reagent. Biomass Bioenerg. https://doi.org/https://doi.org/10.1016/S0961-9534(02)00135-6.

I. Calizo, A.A. Balandin, W. Bao, et al., 2007. Temperature dependence of the Raman spectra of graphene and graphene multilayers,. Nano. Lett. https://doi.org/https://doi.org/10.1021/nl071033g

Chen, J., Li, G., Huang, Y., et al, 2012. Optimization synthesis of carbon nanotubes-anatase TiO$_2$ composite photocatalyst by response surface methodology for photocatalytic degradation of gaseous styrene. Appl. Catal. B: Environ. 123–124, 69–77. https://doi.org/10.1016/j.apcatb.2012.04.020.

Chen, F., Xie, S., Huang, X., et al, 2017. Ionothermal synthesis of Fe$_3$O$_4$ magnetic nanoparticles as efficient heterogeneous Fenton-like catalysts for degradation of organic pollutants with H$_2$O$_2$. J Hazard Mater. 322, 152–162. https://doi.org/10.1016/j.jhazmat.2016.02.073.

Cooper, C. J., S. Alam, V. d. P. N. Nziko, et al., 2020. Co(salen)-Catalyzed Oxidation of Lignin Models to Form Benzoquinones and Benzaldehydes: A Computational and Experimental Study. ACS Sustainable Chemistry & Engineering. 8, 7225-7234. https://doi.org/10.1021/acssuschemeng.0c01970.

Cuong, T.V., Pham, V.H., Tran, Q.T., et al, 2010. Photoluminescence and Raman studies of graphene thin films prepared by reduction of graphene oxide. Mater. Lett. 64, 399–401. https://doi.org/10.1016/j.matlet.2009.11.029.

Deng, H., Yin, J., Ma, J., et al, 2021. Exploring the enhanced catalytic performance on nitro dyes via a novel template of flake-network Ni-Ti LDH/GO in-situ deposited with Ag$_3$PO$_4$ NPs. Appl. Surf. Sci. 543. https://doi.org/10.1016/j.apsusc.2020.148821.

Fernandez-Fueyo, E., Ruiz-Duenas, F.J., Ferreira, P., et al, 2012. Comparative genomics of Ceriporiopsis subvermispora and Phanerochaete chrysosporium provide insight into selective ligninolysis.

Proc. Natl. Acad. Sci. U. S. A. 109, 5458–5463. https://doi.org/10.1073/pnas.1119912109.

A.C. Ferrari and J. Robertson, 2000. nterpretation of Raman spectra of disordered and amorphous carbon,. Phy. Rev. B. https://doi.org/https://doi.org/10.1103/PhysRevB.61.14095

Ferrari, A.C., Meyer, J.C., Scardaci, V., et al, 2006. Raman spectrum of graphene and graphene layers. Phys. Rev. Lett. 97,. https://doi.org/10.1103/PhysRevLett.97.187401 187401.

Graf, , D., F. Molitor, , K. Ensslin, , et al., 2007. Spatially resolved Raman spectroscopy of single- and few-layer graphene, . Nano. Lett. . https://doi.org/https://doi.org/10.1021/nl061702a

Guan, H., Zhu, L., Zhou, H., et al, 2008. Rapid probing of photocatalytic activity on titania-based self-cleaning materials using 7-hydroxycoumarin fluorescent probe. Anal. Chim. Acta 608, 73–78. https://doi.org/10.1016/j.aca.2007.12.009.

Guo, R., Jiao, T., Li, R., et al, 2017. Sandwiched Fe_3O_4/carboxylate graphene oxide nanostructures constructed by layer-by-layer assembly for highly efficient and magnetically recyclable dye removal. ACS Sustain. Chem. Eng. 6, 1279–1288. https://doi.org/10.1021/acssuschemeng.7b03635.

Ha, J.-M., Hwang, K.-R., Kim, Y.-M., et al, 2019. Recent progress in the thermal and catalytic conversion of lignin. Renew. Sustain. Energy Rev. 111, 422–441. https://doi.org/10.1016/j.rser.2019.05.034.

Han, W. and M. Gao, 2008. Investigations on Iron Sulfide Nanosheets Prepared via a Single-Source Precursor Approach. Cryst. Growth Des. https://doi.org/https://doi.org/10.1021/cg701075u

Hazime, R., Nguyen, Q.H., Ferronato, C., et al, 2013. Optimization of imazalil removal in the system $UV/TiO_2/K_2S_2O_8$ using a response surface methodology (RSM). Appl. Catal. B: Environ. 132–133, 519–526. https://doi.org/10.1016/j.apcatb.2012.12.021.

Hou, X., Huang, X., Jia, F., et al, 2017. Hydroxylamine promoted goethite surface fenton degradation of organic pollutants. Environ. Sci Technol. 51, 5118–5126. https://doi.org/10.1021/acs.est.6b05906.

Huang, X., Chen, Y., Walter, E., et al, 2019. Facet-specific photocatalytic degradation of organics by heterogeneous fenton chemistry on hematite nanoparticles. Environ. Sci. Technol. 53, 10197–10207. https://doi.org/10.1021/acs.est.9b02946.

W. Hummers and R. Offeman, 1958. Preparation of graphitic oxide. J. Am. Chem. Soc. . https://doi.org/https://doi.org/10.1021/ja01539a017

Jiang, G., Lin, Z., Zhu, L., et al, 2010. Preparation and photoelectrocatalytic properties of titania/carbon nanotube composite films. Carbon 48, 3369–3375. https://doi.org/10.1016/j.carbon.2010.05.029.

Jiménez, V., Panagiotopoulou, P., Sánchez, P., et al, 2011. Synthesis and characterization of ruthenium supported on carbon nanofibers with different graphitic plane arrangements. Chem. Eng. J. 168, 947–954. https://doi.org/10.1016/j.cej.2011.02.024.

Kansal, S.K., Singh, M., Sud, D., 2008. Studies on TiO_2/ZnO photocatalysed degradation of lignin. J Hazard. Mater. 153, 412–417. https://doi.org/10.1016/j.jhazmat.2007.08.091.

Kong, L., Yan, L., Qu, Z., et al, 2015. β-Cyclodextrin stabilized magnetic Fe_3S_4 nanoparticles for efficient removal of Pb(ii). J. Mater. Chem. A 3, 15755–15763. https://doi.org/10.1039/c5ta03442f.

Laurichesse, S., Avérous, L., 2014. Chemical modification of lignins: towards biobased polymers. Prog. Polym. Sci. 39, 1266–1290. https://doi.org/10.1016/j.progpolymsci.2013.11.004.

Ma, Y.S., Chang, C.N., Chiang, Y.P., et al, 2008. Photocatalytic degradation of lignin using Pt/TiO_2 as the catalyst. Chemosphere 71, 998–1004. https://doi.org/10.1016/j.chemosphere.2007.10.061.

Ma Li Hua and Wan Jin Quan, 2013. Degradation of Organic Pollutants in Papermaking Wastewater by $Fe^{2+}/S_2O_8^{2-}-H_2O_2$ Deap Treatment System. Paper Science & Technology. 2013, https://doi.org/10.1016/j.cej.2011.02.024

Martin, S.T., Lee, A.T., Hoffmann, M.R., 1995. Chemical mechanism of inorganic oxidants in the TiO_2/UV process: increased rates of degradation of chlorinated hydrocarbons. Environ. Sci. Technol. 29, 2567–2573. https://doi.org/10.1021/es00010a017.

Mei, J., Shen, X., Gang, L., et al, 2020. A novel lignin degradation bacteria-Bacillus amyloliquefaciens SL-7 used to degrade straw lignin efficiently. Bioresour. Technol. 310,. https://doi.org/10.1016/j.biortech.2020.123445 123445.

Pandey, M.P., Kim, C.S., 2011. Lignin depolymerization and conversion: a review of thermochemical methods. Chem. Eng. Technol. 34, 29–41. https://doi.org/10.1002/ceat.201000270.

Parpot, P., Bettencourt, A.P., Carvalho, A.M., 2000. Attempted electronxidation of lignin for vanillin production 2000. J. Appl. Electrochem. 30 (2000), 727–731. https://doi.org/10.1023/A:1004003613883.

Qian, X., Ren, M., Zhu, Y., et al, 2017. Visible light assisted heterogeneous fenton-like degradation of organic pollutant via alpha-FeOOH/mesoporous carbon composites. Environ. Sci. Technol. 51, 3993–4000. https://doi.org/10.1021/acs.est.6b06429.

Rickard, D. and G. W. Luther, 2007. Chemistry of iron sulfides. Chem. Rev. . https://doi.org/https://doi.org/10.1021/cr0503658

Rocha, E.M.R., Vilar, V.J.P., Fonseca, A., et al., 2011. Landfill leachate treatment by solar-driven AOPs. Sol. Energy 85, 46–56. https://doi.org/10.1016/j.solener.2010.11.001.

Roldan, A., de Leeuw, N.H., 2016. Methanol formation from CO_2 catalyzed by $Fe_3S_4\{111\}$: formate versus hydrocarboxyl pathways. Faraday Discuss. 188, 161–180. https://doi.org/10.1039/c5fd00186b.

M.W.I. Schmidt, H. Knicker, P.G. Hatcher, et al., 1997. Does ultrasonic dispersion and homogenization by ball milling change the chemical structure of organic matter in geochemical samples-a ^{13}C NMR study with lignin. Org. Geochem. https://doi.org/https://doi.org/10.1016/S0146-6380(97)00047-8

Sen, S.K., Raut, S., Gaur, M., et al, 2020. Biodegradation of lignin from pulp and paper mill effluent: optimization and toxicity evaluation. J. Hazard., Toxic, Radioact. Waste 24. https://doi.org/10.1061/(asce)hz.2153-5515.0000522.

Shi, Y., Wang, X., Liu, X., et al, 2020. Visible light promoted Fe_3S_4 Fenton oxidation of atrazine. Appl. Catal. B: Environ. 277. https://doi.org/10.1016/j.apcatb.2020.119229.

Song, W., Li, J., Wang, Z., et al, 2020. Degradation of bisphenol A by persulfate coupled with dithionite: Optimization using response surface methodology and pathway. Sci. Total Environ. 699,. https://doi.org/10.1016/j.scitotenv.2019.134258 134258.

Sulaiman, N. F., W. A. Wan Abu Bakar, S. Toemen, et al., 2019. In depth investigation of bi-functional, $Cu/Zn/\gamma-Al_2O_3$ catalyst in biodiesel production from low-grade cooking oil: Optimization using response surface methodology. Renewable Energy. 135, 408–416. https://doi.org/10.1016/j.renene.2018.11.111.

Sun, M., Chu, C., Geng, F., et al, 2018. Reinventing Fenton chemistry: iron oxychloride nanosheet for pH-insensitive H_2O_2 activation. Environ. Sci. Technol. Lett. 5, 186–191. https://doi.org/10.1021/acs.estlett.8b00065.

Suter, J.L., Sinclair, R.C., Coveney, P.V., 2020. Principles governing control of aggregation and dispersion of graphene and graphene oxide in polymer melts. Adv. Mater. 32, e2003213.

Thakur, D.B., Tiggelaar, R.M., Gardeniers, J.G.E., et al, 2010. Carbon nanofiber based catalyst supports to be used in microreactors: synthesis and characterization. Chem. Eng. J. 160, 899–908. https://doi.org/10.1016/j.cej.2010.01.005.

Torrades, F., Saiz, S., García-Hortal, J.A., 2011. Using central composite experimental design to optimize the degradation of black liquor by Fenton reagent. Desalination 268, 97–102. https://doi.org/10.1016/j.desal.2010.10.003.

Tung, V.C., Allen, M.J., Yang, Y., et al, 2009. High-throughput solution processing of large-scale graphene. Nat. Nanotechnol. 4, 25–29. https://doi.org/10.1038/nnano.2008.329.

Vilar, V.J., Maldonado, M.I., Oller, I., et al, 2009. Solar treatment of cork boiling and bleaching wastewaters in a pilot plant. Water Res. 43, 4050–4062. https://doi.org/10.1016/j.watres.2009.06.019.

Wang, M., Zhang, B., Cai, C., et al, 2018. Acidic hydrothermal treatment: Characteristics of organic, nitrogen and phosphorus releasing and process optimization on lincomycin removal from lincomycin mycelial residues. Chem. Eng. J. 336, 436–444. https://doi.org/10.1016/j.cej.2017.12.041.

Xin, S., Liu, G., Ma, X., et al, 2021. High efficiency heterogeneous Fenton-like catalyst biochar modified $CuFeO_2$ for the degradation of tetracycline: economical synthesis, catalytic performance and mechanism. Appl. Catal. B: Environ. 280. https://doi.org/10.1016/j.apcatb.2020.119386.

Xu, L., Wang, J., 2012. Magnetic nanoscaled Fe_3O_4/CeO_2 composite as an efficient Fenton-like heterogeneous catalyst for degradation of 4-chlorophenol. Environ. Sci. Technol. 46, 10145–10153. https://doi.org/10.1021/es300303f.

Xu, Y., Wang, R., Wang, J., et al, 2021. Facile fabrication of molybdenum compounds (Mo_2C, MoP and MoS_2) nanoclusters supported on N-doped reduced graphene oxide for highly efficient hydrogen evolution reaction over broad pH range. Chem. Eng. J. 417. https://doi.org/10.1016/j.cej.2021.129233.

Yang, X.J., Xu, X.M., Xu, J., et al, 2013. Iron oxychloride (FeOCl): an efficient Fenton-like catalyst for producing hydroxyl radicals in degradation of organic contaminants. J. Am. Chem. Soc. 135, 16058–16061. https://doi.org/10.1021/ja409130c.

Yeber, , M. C., J. Rodríguez, J. Freer, , et al., 2000. Photocatalytie degradation of cellulose bleaching e.uent by supported TiO_2 and ZnO. https://doi.org/https://doi.org/10.1016/s0045-6535(99)00551-2.

Zhang, Z.J., Chen, X.Y., 2009. Magnetic greigite (Fe_3S_4) nanomaterials: shape-controlled solvothermal synthesis and their calcination conversion into hematite (α-Fe_2O_3) nanomaterials. J. Alloy. Compd. 488, 339–345. https://doi.org/10.1016/j.jallcom.2009.08.127.

Zhang, B., Chen, M., Li, D., et al, 2020. Quantitative investigation into the enhancing utilization efficiency of H_2O_2 catalyzed by FeOCl under visible light. J. Photochem. Photobiol. A: Chem. 386. https://doi.org/10.1016/j.jphotochem.2019.112072.

Zhao, X., Lan, X., Yu, D., et al, 2018. Deep eutectic-solvothermal synthesis of nanostructured Fe_3S_4 for electrochemical N_2 fixation under ambient conditions. Chem. Commun. (Camb). 54, 13010–13013. https://doi.org/10.1039/c8cc08045c.